



Is there any health danger by radioactivity on the use of dimensional stones?

Siegfried Siegesmund¹ · Alcides Pereira² · Luís Sousa³ · Stine Rucker¹ · Leander Kallas¹ · Bernd Kopka⁴ · Filipa Domingos² · Sérgio Seco²

Received: 19 January 2022 / Accepted: 2 June 2022 / Published online: 20 July 2022
© The Author(s) 2022

Abstract

Natural building stones must be analysed according to a legally defined procedure to prove that the natural radioactivity they emit is below the so-called activity index given by European Commission. This applies in particular to rooms inside buildings or apartments that are used by people for longer periods of time. Gamma spectrometric measurements were determined for all nuclides involved, ⁴⁰K, ²²⁶Ra and ²³²Th, which were finally summed up to a total dose for each sample. Measurements are prescribed to check whether the reference value of 1 milli-Sievert per year can be exceeded by radionuclides in the respective building materials. Natural stones, 82 in total from all over the world, such as various igneous, metamorphic and sedimentary rocks, which are currently used as building stones for interior and exterior finishing, as kitchen worktops, floor tiles, wall cladding, table tops, furniture cover plates, paving stones, terrace slabs, paving slabs, stairs, street furniture, etc., were selected. Additionally, Rn-222 and Rn-220 exhaled per unit mass were determined simultaneously on 54 selected from the total 82 rocks by using the accumulation method. In addition, our results were statistically compared with literature data, according to which fescic igneous rocks, gneisses and clay mineral-rich rocks have the highest potential to be radiologically threatening. Limestones, marbles, quartzites, mafic igneous rocks and sandstones are generally less radiologically harmful, but even here there are exceptions depending on the geological formation history and mineralogical composition. The highest activity index of 1.87 was determined for the gneiss Giallo California. Model calculations to determine the expected radiation exposure for a human were used by applying two less complex approaches. Even with the extreme model “cof-fin”, which consists of the Giallo California, a human experiences only a maximum dose rate of 1.29 mSv a⁻¹, which is far below the maximum dose rate of 20 mSv a⁻¹ allowed for occupational radiation exposure. The ²²⁰Rn and ²²²Rn are often neglected; however, their contribution to the dose rate received by the population may be significant. Model simulations for a room with 4 m × 3 m × 2.5 m where the walls and the floor covered with tiles of 1 cm thickness show a maximum indoor radon concentration of less than 100 Bq m⁻³. With increase in thickness of the tiles up to 3 cm, 10 cm and 20 cm and for poorly ventilated rooms especially some granitoids, gneisses and the copper-rich shale are above the allowed limit of the European Commission.

Keywords Natural stones · Radioactivity · Activity index · Radon exhalation

This article is part of a Topical Collection in Environmental Earth Sciences on “Building Stones and Geomaterials through History and Environments – from Quarry to Heritage. Insights of the Conditioning Factors”, guest edited by Siegfried Siegesmund, Luís Manuel Oliveira Sousa, and Rubén Alfonso López-Doncel.

✉ Siegfried Siegesmund
ssieges@gwdg.de

¹ GZG-Structural Geology and Geodynamics, University of Göttingen, Goldschmidtstr 3, 37077 Göttingen, Germany

² LRN-Laboratory of Natural Radioactivity, Department of Earth Sciences, University of Coimbra, Coimbra, Portugal

³ Department of Geology and Pole of CGeo-Geoscience Center, University of Trás-os-Montes e Alto Douro (UTAD), Vila Real, Portugal

⁴ Labor für Radioisotope, Universität Göttingen, Büsungenweg 2, 37077 Göttingen, Germany

Introduction

Natural stone is a popular construction material, which is used worldwide as a building stone for the outdoor and indoor applications [e.g. (Siegesmund and Sneathlage 2014; Siedel and Siegesmund 2014; Siegesmund and Török 2014)]. They are used there, among other things, as kitchen

tops, floor and wall tiles and for the design of highly exclusive bathrooms, such as shower trays and its wall or floor cladding (Fig. 1). After recurring reports of potentially dangerous radioactive exposure from natural building blocks in indoor environments have been discussed in scientific papers, but also in more popular scientific articles or in quite populist way in newspapers (e.g. Murphy 2008), various studies have been conducted on this topic in recent

Fig. 1 Some examples of the use of stone: **a** Granite houses in Monsanto (Portugal) built directly between the large boulders, **b** typical mountain farmhouse in the Alps built including the roofing of granites, gneisses and mylonites, **c** the Flossenburg granite (Germany) including the castle on the top of hill, **d** shower completely clad with slabs of Black Cosmic (photo D.Drossel), **e** massive rock table of Dorfer Grün (Austria), **f** rock storehouse with a large collection slabs



years (e.g. WHO 2009; Anjos et al. 2011; Pereira et al. 2012; Turhan et al. 2015; De With et al. 2018), including some focussing on kitchen countertops and tiles (e.g. Joel et al. 2018; Myatt et al. 2010; Tzortzis et al. 2003). These have shown that the majority of materials studied are below established European Commission dose limits (Myatt et al. 2010).

Radioactive radiation is expressed in units of Becquerel (Bq) and Grey (Gr) or milli-Sievert (mSv). The unit Bq is used for the intensity of a radiation source, while the unit mSv is an equivalent dose for radiation exposure, since radiation does not affect humans uniformly. A distinction must be made between the body dose (Sv) and the absorbed dose (Grey). The unit Grey describes only the absorbed dose rate, while Sv describes the extent of this absorbed dose rate on the human body. Every day, humans are exposed to a certain amount of natural radioactive radiation and radon from the environment (Deutscher Naturwerkstein-Verband 2019). These natural radioactive radiations include cosmic, terrestrial and intracorporeal radiation. In addition, there is artificial man-made radiation. The German Natural Stone Association (DNV 2019) estimates the average equivalent doses in Germany to be about 0.6–0.9 mSv a⁻¹ (cosmic), about 0.4–2.0 mSv a⁻¹ (terrestrial) and depending on the source of the artificial radiation, it can be, for example, up to 1 mSv for an X-ray examination and even more than 10 mSv for a single computer tomography. Intracorporeal radiation is caused mainly by inhalation of the radioactive gases, radon (²²²Rn), from the decay series of uranium, and, in a much lesser extent, thoron (²²⁰Rn) and, in both cases, by the short-lived decay products (European Commission 1999). Radiation exposure from building materials is divided into external and internal exposure. Here, the external exposure includes direct gamma radiation, and the internal exposure includes the intracorporeal radiation caused mainly by radon inhalation, as mentioned above (European Commission 1999). The “European Commission Report 112” has set a limit for the radioactive radiation of building blocks, which may exceed 1 mSv a⁻¹ only in absolute exceptional cases to be approved separately. For building blocks with a radiation exposure between 0.3 and 1 mSv a⁻¹, a check of the material is recommended. For individuals from the German population, the limit value of 1 mSv a⁻¹ applies (European Commission 1999; Bundesamt für Strahlenschutz 2020); for individuals who are occupationally exposed to radiation, a limit value of 20 mSv a⁻¹ applies (European Commission 1999, Bundesamt für Strahlenschutz). A person from the German population is exposed to an average radiation level of 2–3 mSv a⁻¹ due to natural sources (Bundesamt für Strahlenschutz 2020).

The activity index “I” was presented in 1999 and refers to the activity concentrations of radium (C_{Ra}), thorium (C_{Th}) and potassium (C_K) in the building material to be assessed in Bq kg⁻¹ (European Commission Report 112). The dose

criteria of 0.3 mSv a⁻¹ and 1.0 mSv a⁻¹ are, respectively, equivalent to an activity index of $I \leq 2$ and $I \leq 6$. The activity index is useful to categorize the tested materials as $I \leq 2$, $I \leq 6$, or greater and has been applied in many studies (Joel et al. 2018; Markkanen 1995; Zeghib et al. 2016). If a material is classified as critical according to this index, more accurate dose measurements should be performed.

A limit of 300 Bq m⁻³ is recommended for indoor radon levels, and a typical value for radon concentration that can be caused by indoor building materials is 10–20 Bq m⁻³, but in rare cases it can increase up to 1000 Bq m⁻³ (European Commission 1999).

In the last years, several researches were conducted regarding the evaluation of the radioactivity from rocks and building materials, assessing the contribution of the outcrops for the background radioactivity and potential hazard from building stones and other materials (Ngachin et al. 2008; Nuccetelli et al. 2012; Trevisi et al. 2012; Sayin 2103; Richter et al. 2013; Pereira et al. 2017; Pillai et al. 2017; Guillén et al. 2018; Shohda et al. 2018; Lyngkhoi and Nongkynrih 2020).

The radioactivity of the samples is related with mineralogical composition. Therefore, large variations can be expected considering the rock types and the content of radioactive accessory minerals (Marocchi et al. 2011; Pereira et al. 2013; Sanjurjo-Sánchez and Alves 2017; Maden et al. 2019). Several compilations of concentration values can be found in literature, which emphasizes the natural variations among the rocks (Pereira et al. 2012; Turhan 2012; Trevisi et al. 2012; Sayin 2013; Qureshi et al. 2014; Puccini et al. 2014; Todorovic et al. 2015; Sanjurjo-Sánchez and Alves 2017; Al-Hamarneh 2017; Moghazy et al. 2021).

The available results of the activity concentration index “I” in building stones showed values often below 2 (Trevisi et al. 2012; Puccini et al. 2014; Todorovic et al. 2015; Guillén et al. 2018; El-Gamal et al. 2018), which implies that they can be used as “superficial and other material with restricted uses”, as countertops, tiles, etc. However, some stones depict values higher than 6 limiting their use as building stones (Trevisi et al. 2012).

To a precise evaluation of the radiological risk besides the I index, it is very important to know also the potential of exhalation of the radioactive gases produced in the ²³⁸U and ²³²Th decay chains. This parameter is related not only with the radium source but also other variables as the emanation rate from the minerals and the air permeability of the rocks (Khan 2014); the weathering of the rocks will be another factor to take in account as usually contribute to increase the exhalation rate (Domingos and Pereira 2018; Pereira et al. 2012; El-Gamal et al. 2018). When the volume of material applied is low, as is the case of countertops, the radon concentration originated is not problematic. Allen et al. (2013) simulated one million of countertop purchases and

assessed the resulting radon concentration indoor considering the probability that a particular type of granite would be purchased, the radon emission of that type, the size of the pieces, the volume of the house and the air change rate. They found a median predict value of 0.06 Bq m^{-3} , which is around 2500 times lower than the US Environmental Protection Agency's limit for indoor radon (148 Bq m^{-3}) (US EPA 1993). Therefore, there is a low probability of a building stone used as countertop causing elevated levels of radon. However, when it is used in larger areas, like pavements and/or wall coverings, or in bulk, caution is needed. The ventilation rate is another factor that can influence the indoor radon/thoron concentrations. Martins et al. (2016) found highest indoor radon average values in dwellings with less than 50 years old and basement built in granitic areas. Older dwellings have constructions features, i.e. thermal leaks, making them naturally ventilated. Syuryavin et al. (2020) mentioned a decrease in the effective dose of about 66 times when the air exchange rate increases from 0.00 to 0.50 h^{-1} . Therefore, it is generally accepted that radon concentration in dwellings is more related with natural (lithological) and anthropogenic (constructions features) than the building stones (García-Talavera et al. 2013; Martins et al. 2016).

Despite this last statement and the research done so far, an integrate approach is needed, based on the direct measurements of the control parameters of the radiation sources in the building stones, combined with modelling techniques to evaluate the contributions of its use in different scenarios, with the ultimate goal to evaluate precisely the radiological impacts on the population. This has been done in the present work using as the research object several dozens samples of some of the most used rocks as building stones in the world.

Rock samples—mineralogy

For this study, a wide range of samples were selected regarding the mineralogy and the geological background focussing on ornamental stones but in addition samples which expected higher radiation values were also included. These include acidic, igneous rocks such as granite and a larger variety of metamorphic rocks as well sedimentary rocks. A high organic content in the rock, as can occur in shales and limestones, is also often a source of the relevant radioactive isotopes of uranium, thorium and potassium (Bone et al. 2017; Fuller et al. 2020; Tzortzis et al. 2003; Yang et al. 2012). Based on this finding, a selection of 82 rocks was chosen to measure their radioactivity and calculate the resulting annual equivalent doses and radon exhalation.

For further evaluation (see Table 1), the samples with similar petrographical and geochemical characteristics were divided into eight different rock groups (Fig. 2): (1)

the mafic volcanics/magmatites (basalt, gabbro, trachyandesite and ignimbrite) and their metamorphic equivalents (amphibolite and serpentinite) with a total of seven samples (MV), (2) gneisses (gneiss and kinzingite) with 15 samples (GN), (3) the felsic volcanic rocks/magmatites (granite and granodiorite) with 17 samples (FV), (4) limestones (limestone, travertine) with ten samples (KS), (5) marbles with seven samples (MA), (6) quartzite with five samples (QT), (7) sandstones and similar sedimentary rocks (sandstone, greywacke, metaconglomerate and metapsammite) with nine samples (SA) and (8) metamorphic rocks like slates, phyllites and metapelite with 12 samples (SF).

Potassium is most abundant in rock-forming minerals and has an average concentration of 2.09 wt% (Taylor 1964) or 400 Bq kg^{-1} (European Commission 1999) in the continental crust. Potassium is geochemically an incompatible LILE (large-ion lithophile element), but occurs as a major component in many minerals, such as feldspars (orthoclase, microcline and sanidine), mica and clay minerals (biotite, muscovite, phlogopite and illite), foids (leucite and nepheline) and salts (sylvin). A substitution process often takes place between potassium and sodium, which have geochemically similar properties, in the minerals. Potassium has three isotopes, of which only ^{40}K is radioactive and occurs with a relative abundance of 0.012% (Plant and Saunders 1996) and a half-life of 1.31 Ga (Burch 1953).

Thorium occurs in rocks as a trace element with an average concentration of 9.6 ppm or 40 Bq kg^{-1} in the continental crust (European Commission 1999; Taylor 1964). Thorium occurs in higher concentrations in thorite (in the wt% range) but also in higher trace concentrations in monazite, apatite or allanite, etc. (Frondel and Fleischer 1952). There is a close geochemical relationship between uranium and thorium, both of which are HFSE (high field strength element), in which thorium can partially replace uranium in minerals. Unlike uranium (U^{6+}), thorium is an immobile element. Thorium has only one isotope, ^{232}Th , which is relevant for measuring radioactivity (Plant and Saunders 1996) and has a half-life of 14.2 Ga (Chikkur and Umakantha 1977).

Radium is a highly incompatible element in minerals and has a concentration of about 0.9 ppm, or 40 Bq kg^{-1} in the continental crust (European Commission 1999; Lide 2008). The radium isotope ^{226}Ra is an intermediate decay product of the ^{238}U series with a half-life of 1600 years (Broecker et al. 1967) and is selectively absorbed in clay minerals (e.g. in illite) and metal oxides (Hidaka et al. 2007; IAEA 2014). According to geochemical compatibility, radium is able to substitute in small amounts barium, lead and, to some extent, strontium and calcium, in a crystal lattice. Since in the decay series of ^{238}U - ^{206}Pb the segment beginning with ^{226}Ra is radiologically the most important, the activity of radium is

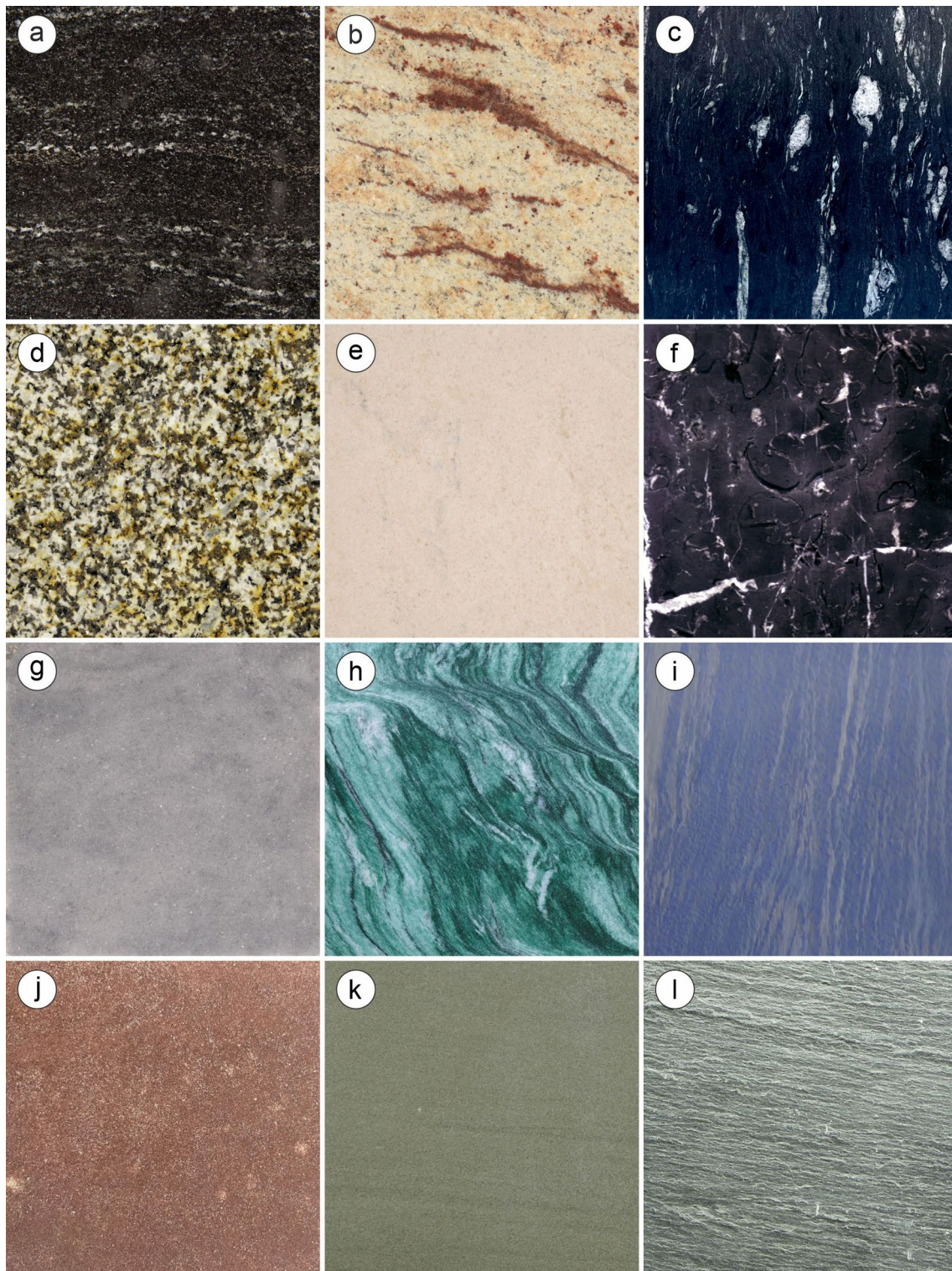


Fig. 2 Macroscopic images of rock varieties belonging to the rock groups: MV—Mafic rocks, GN—gneisses and kinzigites, FV—felsic rocks, KS—limestones and travertines, MA—marbles, QT—quartzites, SA—sandstones and similar sedimentary rocks, SF—metamorphic rocks as given in Table 1 **a** Via Lattea, **b** Shivakashi, **c** Black

Cosmic, **d** Flossenbürg, **e** Vratza, **f** Negro Marquina, **g**, Ruvina, **h** Masi, **i** Azul Macauba, **j** Tambach Sandstone, **k** Schleerith, **l** San Luis slate. For a better readability, the different rock groups have been given colour coded and this has been used accordingly in all other figures

samples were sealed airtight with adhesive tape and stored for 4 weeks until measurement, to establish radioactive equilibrium of Ra-226 and the follow-on products Rn-222, and especially Pb-214 and Bi-214.

The activity of K-40 was measured directly. The other two radionuclides, Ra-226 and Th-232, show only gamma emissions with low transition probability, which would be partially perturbed by stronger lines of other nuclides. The Ra-226 was determined by the average of the Pb-214 and Bi-214 activities. A secular equilibrium between Ra-226 and Rn-222 is achieved in 23 days (Gehrcke et al. 2012). Similarly, the determination of the activity for Th-232 was calculated by the mean value of Ac-228, Pb-212 and Bi-212. In the two radioactive decay series, the noble gas radon occurs as an intermediate product that can escape from the samples. Because both isotopes of radon have relatively short half-lives (3.82 days for Rn-222 in the uranium decay series and 56 s for Rn-220 in the thorium decay series; Cecil and Green 2000) and the samples were stored in gas-tight beakers, the measured samples are not affected by radon loss. The mean analytical detection limits from all gamma spectrometric measurements were determined as follows: Pb-214 = 1.7091 Bq kg⁻¹, Bi-214 = 1.3103 Bq kg⁻¹, Ac-228 = 2.0377 Bq kg⁻¹, Pb-212 = 0.5281 Bq kg⁻¹, Bi-212 = 6.081 Bq kg⁻¹, K-40 = 6.504 Bq kg⁻¹.

The samples were measured on 3 pure germanium detectors, Canberra N-type with a relative efficiency of about 25%, each for 250,000 s. The electronics with analogue to digital converters were at detector GE1—Ortec Dspec LF, at GE2—Ortec Dspec jr and at GE3—Ortec 92X Spectrum Master.

The obtained raw data were processed with the software Gammavision 8.10 and user interface.

LV is 2.760. Activity calculation from the recorded spectra was performed using the mentioned programs according to DIN 11929 (2020) for determination of detection limit, activity and error.

The background was determined using the same empty sample vessels. The energy and efficiency calibration was performed using the same sample containers filled with quartz sand with a density of 1.6 with added Multi Nuclide Standards.

The activity Index (“I”) proposed in the European Directive (European Commission 1999) was calculated by the following equation:

$$I = \frac{A_{\text{Ra}}}{300 \frac{\text{Bq}}{\text{kg}}} + \frac{A_{\text{Th}}}{300 \frac{\text{Bq}}{\text{kg}}} + \frac{A_{\text{K}}}{3000 \frac{\text{Bq}}{\text{kg}}} \leq 1 \quad (1)$$

Calculation of the equivalent dose

To determine the equivalent doses H (for the explanation see Eq. 4), the free software Rad Pro Calculator (version 3.26) by Ray McGinnis was used. For the calculation, the simplified assumption applies that it is a point source of radioactive radiation. This assumption is made in order to obtain dose rate data for the samples that can be compared with the literature and the legal regulations. When calculating the doses, the first step was to calculate the activities via the measured specific activities and the masses of the substances. Since the dose depends on the distance of the radioactive point source, the calculations were carried out for the distances $s=0.01$ m, $s=0.05$ m and $s=0.1$ m. In this way, the doses for all involved substances were calculated. Thus, the doses were determined for all nuclides involved, ⁴⁰K, ²²⁶Ra and ²³²Th, which were finally summed up to a total dose for each sample. For the samples where the specific activity of the three nuclides was below the detection limit, the activity was assumed to be $A=0$ Bq for the calculation in order to still obtain a quantified value for the dose.

Radon and thoron exhalation rate

Rn-222 and Rn-220 exhaled per unit mass were determined simultaneously with the accumulation method following the procedures described in Domingos et al. (2021). The crushed rock samples were placed in beakers with an approximately volume of 0.3 L. The beakers were then placed in stainless steel radon-proof containers with a volume of 5 L and sealed with a lock ring to prevent radon loss. The containers were left to reach equilibrium in the radon ²²²Rn decay series. Rn-222 and Rn-220 were measured simultaneously with an AlphaGuard DF2000 monitor (from Saphymo GmbH) using Tygon standard LMT-55 tubes characterized by low gas permeability to couple the containers to the measuring equipment. The length of the tubes was minimized to increase the efficiency of Rn-222 recovery.

The AlphaGuard DF2000 monitor continuous Rn/Tn measuring protocol was selected to discriminate between Rn-222 and Rn-220 activity concentration using a flowrate of 2 L/min. The detection limits are 15 Bq/m³ for ²²²Rn and 30 Bq/m³ for ²²⁰Rn (Burkin and Villert 2017). These authors also recommend that the activity concentration to be measured over longer periods to increase the accuracy of the mean results computed. Hence, on average, measurements of the activity concentration of the radioisotopes were performed over a 24 h period with previous subtraction of the background (not taken in account for thoron because of its short half-life). The instrument was decontaminated between each measurement by pumping atmospheric air into the ionization chamber.

The Rn-222 and the Rn-220 exhalation rates (in Bq kg⁻¹ h⁻¹) were determined with the following equation:

$$*Rn = \frac{C \times V}{W \times \lambda} \quad (2)$$

where * is the isotope, *C* is the mean activity concentration (in Bq/m³), *V* is the free volume of the accumulator (in m³), *W* is the weight of the sample (in kg), and *λ* is the decay constant (in h⁻¹). The emanation coefficients (EC) of Rn-222 and Rn-220 were computed with following equation, where *A* is the activity concentration (in Bq/kg) of ²²⁶Ra and ²³²Th, respectively:

$$EC = \frac{C \times V}{W \times A} \times 100 \quad (3)$$

Results

Activity concentration of radionuclides

Within the rock groups, described different levels of activity are observed in the three nuclides measured. The activities of the radionuclides can be seen in Table 1 and in Fig. 3.

Similarities to the literature (Gehrcke et al. 2012) can generally be observed, as most materials show activities *A* < 80 Bq kg⁻¹ for ²²⁶Ra, *A* < 100 Bq kg⁻¹ for ²³²Th and *A* < 400 Bq kg⁻¹ for ⁴⁰K. Thus, the upper limits of normal activities *A* < 100 Bq kg⁻¹ for ²²⁶Ra and ²³²Th and *A* < 1000 Bq kg⁻¹ for ⁴⁰K for construction materials are also met for most samples (European Commission 1999). Within the discussed sample groups, different intensities of activity are observed regarding the three measured nuclides.

A clear contrast is seen between the felsic (FV) and mafic (MV) rocks in terms of Ra activity (FV median = 105.3 Bq kg⁻¹; MV median = 3.9 Bq kg⁻¹) and Th activity (FV median = 50.7 Bq kg⁻¹; MV median = 6.3 Bq kg⁻¹). This can mainly be attributed to the incorporation of uranium and thorium in the crystal lattices of the minerals. In the Earth's mantle and mafic rocks, uranium and thorium occur in relatively low concentrations because they are incompatible in the mafic minerals. During partial melting and fractional crystallization, uranium and thorium are enriched in the melt phase, so they occur in greater concentrations in the more highly differentiated rocks. (IAEA 1989; Larsen and Gottfried 1960). In the metamorphic products of the magmatites (especially in MV), no U- or Th-loss is to be expected due to metamorphic processes, but uranium can be mobilized as U⁶⁺ by hydrothermal processes, while thorium behaves immobile (Dostal and Capedri 1978). Kalium is a less incompatible

element than uranium or thorium, but behaves similarly to other incompatible elements in magmatic differentiation (Tilling and Gottfried 1969). Thus, the difference in K activities between FV (median = 1003 Bq kg⁻¹) and MV (median = 125.3 Bq kg⁻¹) is equally evident. In the mafic rocks, potassium can be incorporated in amphibole, pyroxene or plagioclase in minimal amounts, thus slightly higher activities are also observed for MV (Fig. 3). In the felsic rocks, potassium is incorporated as a major element in mica and potassium feldspar, providing the highest K activities of all groups (Table 1, Fig. 3). In group MV, Trachyandesite from Armenia and Brown Chocolate are characterized by higher Ra, Th and K activities than the rest of the samples. In the FV group, Coral Red has a particularly high activity for Th, whereas Monsoon and Bianco Saviolo have significantly lower Ra activities than the rest of the samples.

In the limestones (KS), the lowest activities are ²²⁶Ra (median = 6.00 Bq kg⁻¹), ²³²Th (median = 0.81 Bq kg⁻¹) and ⁴⁰K (median = 9.68 Bq kg⁻¹). In the marine environment, under oxic conditions, uranium occurs mainly as U⁶⁺ (uranyl), which can be dissolved in water in relatively large amounts. The precipitation of uranium in the larger uranyl-calcium complexes is not excluded, so limestones can have U concentrations in higher trace ranges (Klinkhammer and Palmer 1991). This also explains the variance in the Ra activities of KS. During the formation of travertines, uranium is incorporated as trace from the water into the crystals as soon as the redox conditions change (Schwarcz et al. 1979). Thorium also shows a relatively low activity in the limestones, because thorium is not incorporated into the crystal lattices of the carbonate minerals, but it can be found in the clay or heavy mineral fraction of the limestones (Bayer et al. 1969). Since thorium is an immobile element, it is also not incorporated into the travertines, which allows the dating of travertines using U-Th (Schwarcz et al. 1979). Potassium contents in a limestone are usually low, resulting in relatively low K activities, but they may show some variation. Potassium can be incorporated into the defective sites of the carbonate minerals, between carbonate ions and CaO₆-octahedra, especially at higher-salinity waters (Ishikawa and Ichikuni 1984). In the KS group, the black limestone Uttaradit White Grey from Thailand has relatively high Th and K activities compared to the rest of the samples.

Marbles show low activities of ²²⁶Ra (median = 5.76 Bq kg⁻¹), ²³²Th (median = 0.62 Bq kg⁻¹) and ⁴⁰K (median = 62.60 Bq kg⁻¹). Since marble is mineralogically composed mainly of calcite and dolomite, low concentrations of uranium, thorium and potassium and thus low activities of ²²⁶Ra, ²³²Th and ⁴⁰K are to be expected, similar to limestones. It has been reported that uranium can be incorporated into marble in small amounts during metamorphism in secondary phases (Hamdy and Aly 2011). Similarly, other radioactive nuclides besides uranium can be

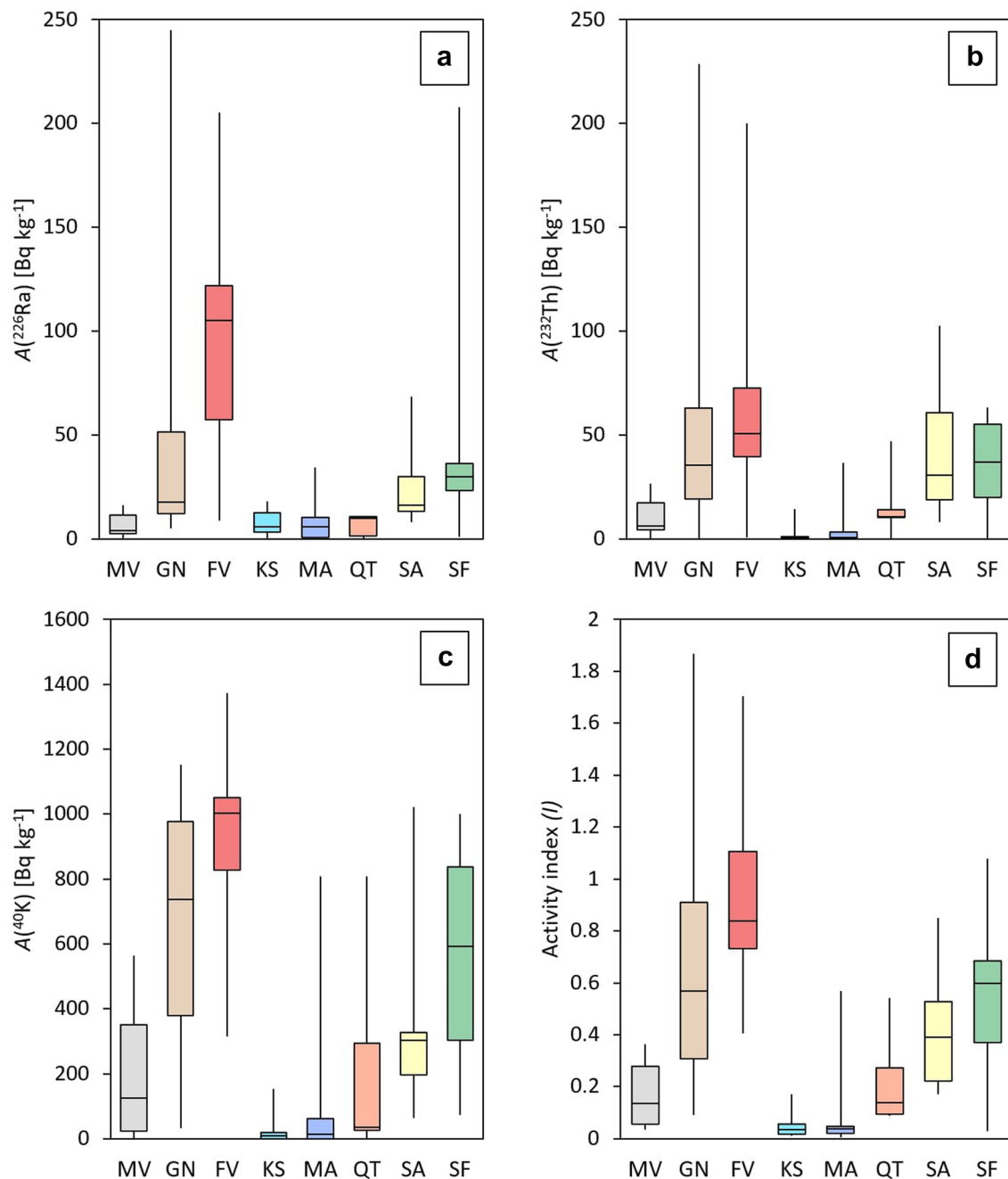


Fig. 3 The statistical summary of the lithological groups is based on the specific activities A in Bq kg^{-1} , shown as boxplots; **a** for ^{226}Ra calculated from ^{214}Pb and ^{214}Bi , **b** for ^{232}Th calculated from ^{228}Ac , ^{212}Bi (and ^{212}Pb) and **c** for ^{40}K directly measured. **d** represents the activity indices of the sample groups. The red line represents the limit of the index ($I=2$), above which the samples require further radiological examinations before use. For the legend, see also Table 1 MV—

mafic rocks (e.g. basalt, gabbro, trachyandesite, amphibolite, serpentinite and ignimbrite); GN—gneisses and kinzingite; FV—felsic rocks (granites and granodiorites); KS—limestones and travertines; MA—marbles; QT—quartzites; SA—sandstones and similar sedimentary rocks (e.g. sandstone, greywacke, metaconglomerate and metapsammite); SF—metamorphic rocks (e.g. slates, phyllites and metapelite)

concentrated in marble, by enriched fluids from uranium-bearing rocks (Iqbal et al. 2000). From group MA, the sample Black Fuao shows strongly high activities for the three measured radionuclides.

In the group of sandstones (SA), moderate variance was observed in the activities of ^{226}Ra (median = 16.37 Bq kg^{-1}) and ^{232}Th (median = 30.69 Bq kg^{-1}), while ^{40}K (median = 304.6 Bq kg^{-1}) shows marked variations. In the

sedimentation of sandstones, the provenance of the sediments plays an important role in their chemical and mineralogical composition. Particularly high uranium concentrations can be measured if the sandstones originate from a felsic magmatic source area (IAEA 1985). Elevated uranium concentrations can also occur in sandstones if reducing components (e.g. organic material, S^{2-}) are present in the groundwater, so that dissolved uranium is reduced to U^{4+} and precipitated as a secondary phase (IAEA 1985; World Nuclear Association 2020). Elevated uranium and thorium contents may be caused by a greater amount of heavy minerals, such as monazite or zircon, in the sandstone, yielding higher Th and Ra activities (Murray and Adams 1958; Rogers and Richardson 1964). Potassium feldspar may occur in sandstones as a major component and is even an important factor in the classification of sandstones (McBride 1963; Pettijohn et al. 1987). Thus, the K content, as well as the activity of ^{40}K , in the sandstones can vary greatly between K-poor quartz sandstones and K-rich arkoses. In the group SA, the sample Tambacher Sandstein shows a particularly high activity of K and the sample Terra Indigo an increased activity of Th.

Quartzite (group QT) is a metamorphic product of sandstone, which mineralogically consists predominantly of quartz. Similar to the sandstones, it shows low activities for ^{226}Ra (median = 10.02 Bq kg $^{-1}$) and ^{232}Th (median = 10.67 Bq kg $^{-1}$), with a higher variance in the activity of ^{40}K (median = 36.41 Bq kg $^{-1}$). Equivalent to sandstones, low concentrations of uranium and thorium are usually expected in a quartzite, with elevated amounts of uranium and thorium often associated with the occurrence of heavy minerals (Jain 1972). In exceptional cases, as with other metamorphic rocks, uranium can be enriched in quartzite via hydrothermal processes, often requiring certain changes in redox conditions (Goswami et al. 2019). Quartzites are usually relatively depleted in potassium due to their high quartz content, although certain mineral phases, such as mica or K-containing clay minerals, can provide higher K concentrations, resulting in higher ^{40}K activities (Lindeman et al. 2020). In the QT group, the Vasa quartzite sample has a high K activity, and the Masi quartzite sample has very high K and Th activities.

The clayey rocks (group SF) show a very high variance of the activities of ^{226}Ra (median = 29.92 Bq kg $^{-1}$) and ^{40}K (median = 591.75 Bq kg $^{-1}$), while the activity of ^{232}Th (median = 36.90 Bq kg $^{-1}$) is less scattered. Clay minerals have the ability to incorporate uranium in different ways. The claystones that form in (deep) marine areas would, like limestones, incorporate relatively little uranium and thorium from the water into the crystal lattice. Uranium has a special affinity for organic material and is thus more enriched in sedimentary layers with a high organic content (Cumberland et al. 2016; Klinkhammer and Palmer 1991). In addition,

clay minerals have the ability to efficiently adsorb uranium and, to some extent, thorium on their surfaces, which can also result in an increase in U and Th concentrations (Ames et al. 1983; Syed 1999). The metamorphic products of the mudstones, shales and phyllites are largely composed of different clay minerals, such as illite, vermiculite and chlorite, which may contain high levels of potassium. High initial concentrations of potassium in clay minerals, as well as their ability to exchange with soil potassium, can strongly influence K concentrations in rocks (Inoue 1983; Sawhney 1972). Among the samples of the SF group, the sample of copper shale from the Richtelsdorf Mountains has a very high Ra activity.

The gneisses (group GN) show the broadest spectrum of activities of ^{226}Ra (median = 17.78 Bq kg $^{-1}$), ^{232}Th (median = 35.48 Bq kg $^{-1}$) and ^{40}K (median = 738.3 Bq kg $^{-1}$), because they can form as a metamorphic product of many different rocks under diverse P–T conditions. Thus, the concentrations of uranium, thorium and potassium in the gneiss samples are very dependent on the source rock. Gneisses formed from felsic and intermediate igneous rocks can have high to very high radionuclide activities, similar to the FV group, while gneisses formed from sedimentary rocks tend to have medium to low activities (Heier and Rhodes 1966). Apart from the source rock, the geochemical composition of gneisses also depends strongly on the type of metamorphism, whereby circulating fluids can also influence the concentrations of potassium and uranium. In the GN group, the Shiwakasi sample has a particularly high activity of Ra and the Giallo California sample a high activity of Th.

Using Eq. 1, building materials can first be tested generally for their radiological hazard with I index value (European Commission 1999; Gehrcke et al. 2012; Markkanen 1995). For the solid building materials used, the limits are: $I > 1$ —radiologically hazardous and prohibited (dose of 1 mSv a $^{-1}$); $I > 0.5$ more precise controls are needed (dose of 0.3 mSv a $^{-1}$). Since this set of samples concerns building materials that are to be used only superficially in lower thicknesses, these limits are correspondingly $I > 6$ and $I > 2$. With the maximum value of $I = 1.87$ for the Giallo California sample, no analysed sample exceeds the limit for further control.

No general statements about the radiological hazards of different rocks should be made solely on the basis of lithology, but clear differences can be observed for the different rock groups (Fig. 3, Table 1). The majority of the samples from the groups MV, KS, MA and QT are clearly below $I = 0.5$, while the group SA also exceeds this value with several samples. Groups SF, GN and FV have activity indices mainly in the range $0.5 \leq I \leq 1$, with individual samples having higher indices up to $I = 1.87$. In addition, it should be noted that these groups have a very low activity index. In addition, it should be borne in mind that these natural

stones are installed in households as thinner cover slabs. Thus, significantly lower activity indices of these analysed building materials are to be expected in reality. Thus, the use of these radiologically analysed products should be permitted by law, without further investigations. The activity indices are clearly controlled by the thickness ($d=20$ cm) of the building materials, whereby the distribution of the activity indices at lower thicknesses gives the same pattern with systematically lower values (not shown here but see “Discussion” in European Commission 1999 and Bundesamt für Strahlenschutz 2020).

Radon and thoron exhalation rates and emanation coefficients

Descriptive statistics are presented for ^{222}Rn and ^{220}Rn exhalation rate and their respective emanation coefficients in Tables 1 and 2. ^{220}Rn exhalation rate is higher than ^{222}Rn exhalation rate by an order of magnitude of 3 due to the shorter half-life of ^{220}Rn . ^{222}Rn exhalation rate ranges from 0.002 to 0.440 $\text{Bq kg}^{-1} \text{h}^{-1}$ with a mean of 0.041 $\text{Bq kg}^{-1} \text{h}^{-1}$, whereas ^{220}Rn exhalation rate ranges from 95 to 463 $\text{Bq kg}^{-1} \text{h}^{-1}$ with a mean of 98 $\text{Bq kg}^{-1} \text{h}^{-1}$. The ^{222}Rn emanation coefficient ranges from less than 1 to 40%, averaging 8%, while the ^{220}Rn emanation coefficient ranges from less than 1 to 31%, averaging 5%. ^{222}Rn exhalation rate is more variable than ^{220}Rn exhalation rate, as shown by the larger coefficient of variation. Conversely, the ^{220}Rn emanation coefficient is more variable than ^{222}Rn emanation coefficient. The ratio between ^{222}Rn emanation coefficient and ^{220}Rn emanation coefficient shows that the first is, on average, two times higher than the later.

All variables present a positive skewness larger than 1, indicating strongly asymmetric distributions. The kurtosis is

also larger than the kurtosis of the normal distribution (of 3), indicating strong deviations from the normal distribution. Thus, nonparametric correlation tests such as the Spearman rank correlation coefficient were computed to assess the relationship between ^{222}Rn and ^{220}Rn exhalation rate and their respective emanation coefficients. The results of the Spearman rank correlation indicate a statistically significant correlation between ^{222}Rn and ^{220}Rn exhalation rates ($R=0.40$, p value = 0.006, degrees of freedom = 43) and ^{222}Rn and ^{220}Rn emanation coefficients ($R=0.44$, p value = 0.002) for a significance level of 0.01.

Data were grouped according to sample groups described in Table 1 and Fig. 3. In Fig. 4, the felsic rocks (FV) present the highest median exhalation rates for both ^{222}Rn and ^{220}Rn , followed by metamorphic rocks (SF) such as slates, phyllites and metapelites (Fig. 4a and b). The lowest exhalation rates are observed in mafic rocks (MV), limestones and travertines (KS). Quartzites also present a low median ^{222}Rn exhalation rate compared to other sedimentary rocks and metamorphic rocks (SA and SF groups, respectively); however, their median ^{220}Rn exhalation rate is similar to sedimentary and metamorphic rocks, namely to the SA and SF sample groups. Marbles also present median ^{222}Rn and ^{220}Rn exhalation rates similar to the SF group. Gneisses present a low median ^{222}Rn exhalation rate but high median ^{220}Rn exhalation rate compared to other groups. ^{222}Rn and ^{220}Rn exhalation rates are highly variable in the GN, FV and SF units, as shown by the range of values in the box and whiskers plot (Fig. 4).

The median ^{222}Rn emanation coefficient is only higher than 10% in the SA and QT units. Values for the emanation coefficient generally lower than 30% are in accordance with typical values reported in the literature for a variety of materials (e.g. Sakoda et al. 2011). The lowest median

Table 2 Descriptive statistics of ^{222}Rn and ^{220}Rn exhalation rate and emanation coefficients (see Table 1)

	^{222}Rn exhalation rate ($\text{Bq kg}^{-1} \text{h}^{-1}$)	^{220}Rn exhalation rate ($\text{Bq kg}^{-1} \text{h}^{-1}$)	^{222}Rn emanation coefficient (%)	^{220}Rn emanation coefficient (%)	^{222}Rn emanation coefficient/ ^{220}Rn emanation coefficient
Number of samples ^a	54	46	54	45	44
Mean	0.041	98	8	5	2
Standard deviation	0.080	95	8	5	2
Minimum	0.002	7	< 1	< 1	0
First quartile	0.006	35	3	2	1
Median	0.014	78	6	4	2
Third quartile	0.027	131	11	5	4
Maximum	0.440	463	40	31	12
Coefficient of Variation (%)	196	97	97	105	85
Skewness	4	2	2	4	2
Kurtosis	14	5	5	15	9

^aSamples below the lower limit of detection were excluded. Rn-220 emanation fraction was not determined in samples presenting either a Th-232 activity concentration or a Rn-220 activity concentration below the lower limit of detection

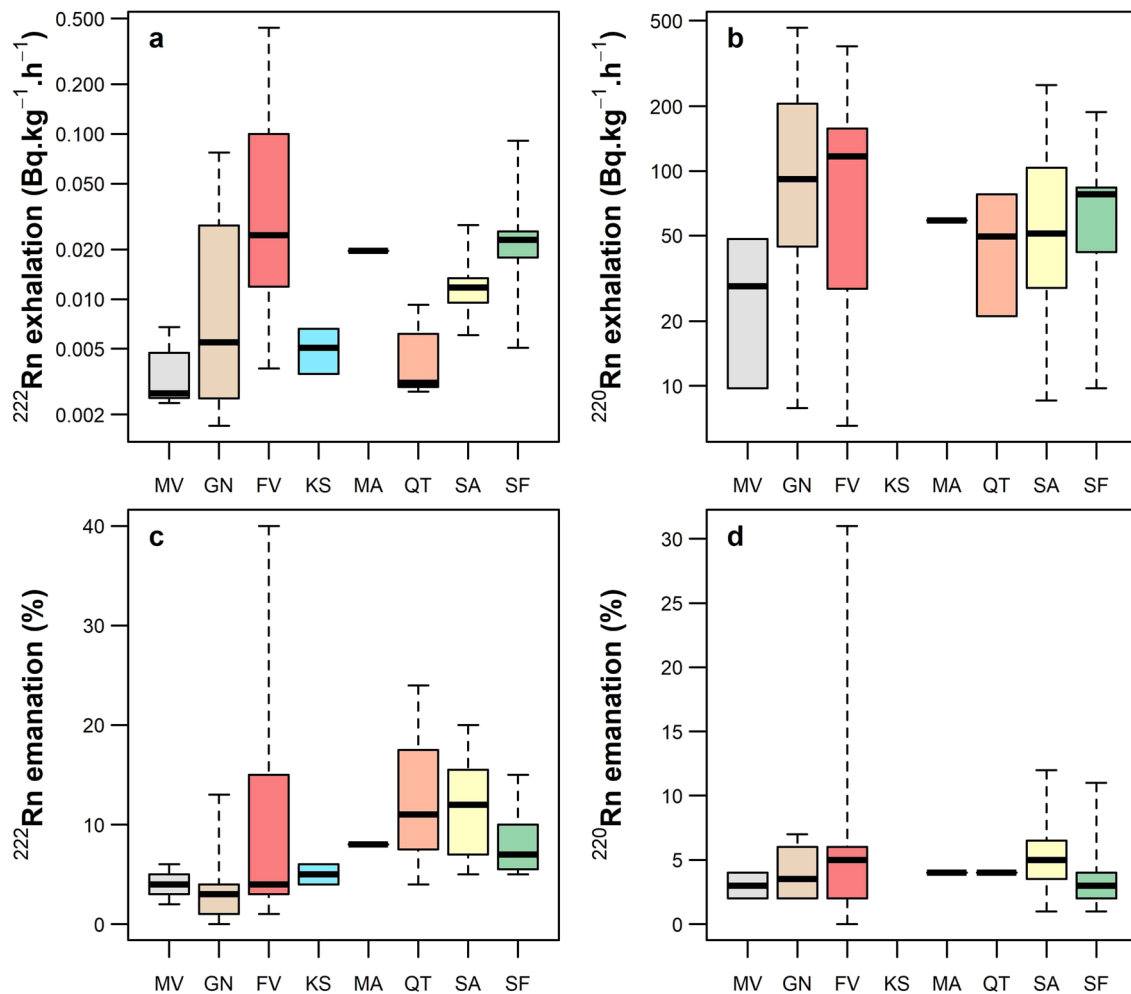


Fig. 4 The statistical summary of the lithological groups shown as boxplots; **a** for ^{222}Rn exhalation rate (in $\text{Bq} \cdot \text{kg}^{-1} \cdot \text{h}^{-1}$), **b** for ^{220}Rn exhalation rate (in $\text{Bq} \cdot \text{kg}^{-1} \cdot \text{h}^{-1}$), **c** for ^{222}Rn emanation coefficient and **d** ^{220}Rn emanation coefficient. The y-axis is in logarithmic scale in plots A and B. Legend: MV—mafic rocks (e.g. basalt, gabbro, trachyandesite, amphibolite, serpentinite and ignimbrite); GN—gneisses

and kinzingite; FV—felsic rocks (granites and granodiorites); KS—limestones and travertines; MA—marbles; QT—quartzites; SA—sandstones and similar sedimentary rocks (e.g. sandstone, greywacke, metaconglomerate and metapsammite); SF—metamorphic rocks (e.g. slates, phyllites and metapelite)

values for the ^{222}Rn emanation coefficient are observed in the GN unit, followed by MV, FV, KS, SF and MA units. The median ^{220}Rn emanation coefficient is fairly similar among sample groups, with median values lower than 10% in all studied units.

The FV unit present the highest variability in terms of both the ^{222}Rn and ^{220}Rn emanation coefficients, and may exceed 30%. Pereira et al. (2017) report median ^{222}Rn emanation values ranging from 19 to over 30% in granitic rocks, much higher than the median values reported in the present work for FV. Domingos and Pereira (2018) report median ^{222}Rn emanation values of 16% for weathered metamorphic rocks, which are also higher than the median values reported

in the present work for the SF unit. However, the increase in the ^{222}Rn emanation values reported by Domingos and Pereira (2018) is linked to the high degree of chemical and physical alteration. Sêco et al. (2020) reported median ^{222}Rn emanation values lower than 24% for sedimentary rocks outcropping in the Lusitanian Basin (Portugal), similarly to the results obtained in the present study (Fig. 4c). The lowest ^{222}Rn emanation values reported by Sêco et al. (2020) correspond to sedimentary rocks presenting a high carbonate fraction, such as limestones, dolostones and dolomitic limestones. In the present study, the lowest ^{222}Rn emanation values are also observed in limestones (KS) when compared to other sedimentary rocks (SA).

Discussion

Radiological assessment of the samples—equivalent doses

The set limits of the activity indices correspond to the limits of the effective doses to which people may be exposed to. According to the principles of radiological safety, all building materials that produce a dose of $H > 1 \text{ mSv a}^{-1}$ must be comprehensively controlled and may only be used in special cases (European Commission 1999; Markkanen 1995). However, it is recommended that products with a dose of $H > 0.3 \text{ mSv a}^{-1}$ also be examined radiologically before use. In Germany, the population may be exposed to a maximum dose of $H = 1 \text{ mSv}$ in a calendar year (European Commission 1999; Bundesamt für Strahlenschutz 2020), whereas occupationally exposed persons may be exposed to a dose of $H = 20 \text{ mSv}$ in a calendar year (European Commission 1999; Bundesamt für Strahlenschutz 2020).

Here, the equivalent doses of the samples were determined in the assumed case with the distance $s = 1 \text{ cm}$ and the exposure time of 8760 h (corresponding to a whole year) for individual radionuclides (Fig. 5a–c), as well as a total sum (Fig. 5d).

The equivalent doses were calculated using specific software, assuming radioactive point sources randomly distributed. A remarkable observation is that with this method the dose values of the nuclide ^{232}Th are several orders of magnitude lower than the doses of ^{226}Ra and ^{40}K . As with the activities, clear differences are observed between the different groups, whereby a generalization by rock type on the basis of the equivalent doses is also not correct, since the data within the groups partly show a strong variance. In the distribution of equivalent doses of the individual nuclides, the patterns of the activity distributions (Fig. 3) can be found again. The proportionality of the doses to the activities has also been reported by Markkanen (1995). For the dose of ^{226}Ra , the MV, KS, MA and QT groups have the lowest values, with the SA group having slightly higher doses and the FV, GN and SF groups having very high scatter and highest doses. For the doses of ^{232}Th , the MV, KS, MA and QT groups also have the lowest values, with SA and SF having slightly higher values with moderate scatter and GN and FV having high doses with strong variance. At ^{40}K , the KS group has the lowest doses, with MV showing slightly increased doses with smaller variance, and the MA, QT and SA groups showing slightly increased doses with greater variance. The groups FV, GN and SF have the highest dose values with the highest variances. The equivalent doses, calculated on $s = 1 \text{ cm}$ spacing, have assumed values between 0 and 2.61 mSv a^{-1} , with a total of 24 samples showing a critical dose of $H > 1 \text{ mSv a}^{-1}$ (three

samples of which, Shiwakashi, Branco Micaela and Waldstein Granite with doses $H > 2 \text{ mSv a}^{-1}$) and theoretically should not be used. As already mentioned, the equivalent dose is strongly dependent on the distance to the radioactive point source, so that the maximum doses of the sample set decrease for $s = 5 \text{ cm}$ to $H_{\text{max}} = 0.10 \text{ mSv a}^{-1}$ and for $s = 10 \text{ cm}$ to $H_{\text{max}} = 0.03 \text{ mSv a}^{-1}$. The dependence of the equivalent dose on the distance from the radioactive source is exemplified for the sample Shiwakashi in Fig. 6, which showed the highest equivalent doses from the whole sample set. The equivalent dose decreases in a quadratic relation to the distance, so that already at $s = 20 \text{ cm}$ hardly any radiation dose is to be expected. The distance $s = 1 \text{ cm}$ was chosen for Fig. 6 because this represents the minimum distance in the calculations at which a number of samples exceeded the legal dose limit of $H = 1 \text{ mSv a}^{-1}$. Since no human being is in this proximity to the slabs and tiles made of these natural stones throughout the year, the radiation from these samples poses no danger and they may be used legally without restrictions.

The samples from the different rock groups classified in Table 1 were compared with the corresponding analytical results from the existing literature and presented in Tables 3, 4, 5, 6, 7, 8, 9, 10. The presented data given in Tables 3, 4, 5, 6, 7, 8, 9, 10 refer to the following references: [1] Bundesamt für Strahlenschutz (2020), [2] Deutscher Naturwerkstein-Verband (2019), [3] Gehrcke et al. (2012), [4] Yalcin et al. (2020), [5] Ahmed et al. (2006), [6] Örgün et al. (2007), [7] El Aassy et al. (2011), [8] Marocchi et al. (2011), [9] Kovler et al. (2002), [10] Madruga et al. (2019), [11] Shohda et al. (2018), [12] Weng (1996), [13] Mohamed et al. (2016), [14] Rafique et al. (2014), [15] Turhan et al. (2009), [16] Aykamis and Kilic (2011), [17] Iqbal et al. (2000), [18] Pereira et al. (2013), [19] Zeghib et al. (2016).

These literature values should only serve as a general classification of the samples used in this study. These literature values do not represent typical activities for the individual rock types. For the comparison, in most cases the median values of the activities A of the individual groups (calculated from Table 1) were determined.

Radiological studies of granites from different locations are very common in the literature, as they often have amount of radiological components and are often used as natural stone slabs (Myatt et al. 2010; Tzortzis et al. 2003). The activities of the granites of ^{226}Ra from the literature range from 39 to $133.31 \text{ Bq kg}^{-1}$, and the median from the granites from this project is located at $105.35 \text{ Bq kg}^{-1}$. The literature values for ^{232}Th activity range from 11.7 to 210 Bq kg^{-1} , while the median of the granites of this project is 50.67 Bq kg^{-1} . In the literature, there is also a wide variation in the activities of ^{40}K between 762.5 and $2012.03 \text{ Bq kg}^{-1}$, with the median value of the studied

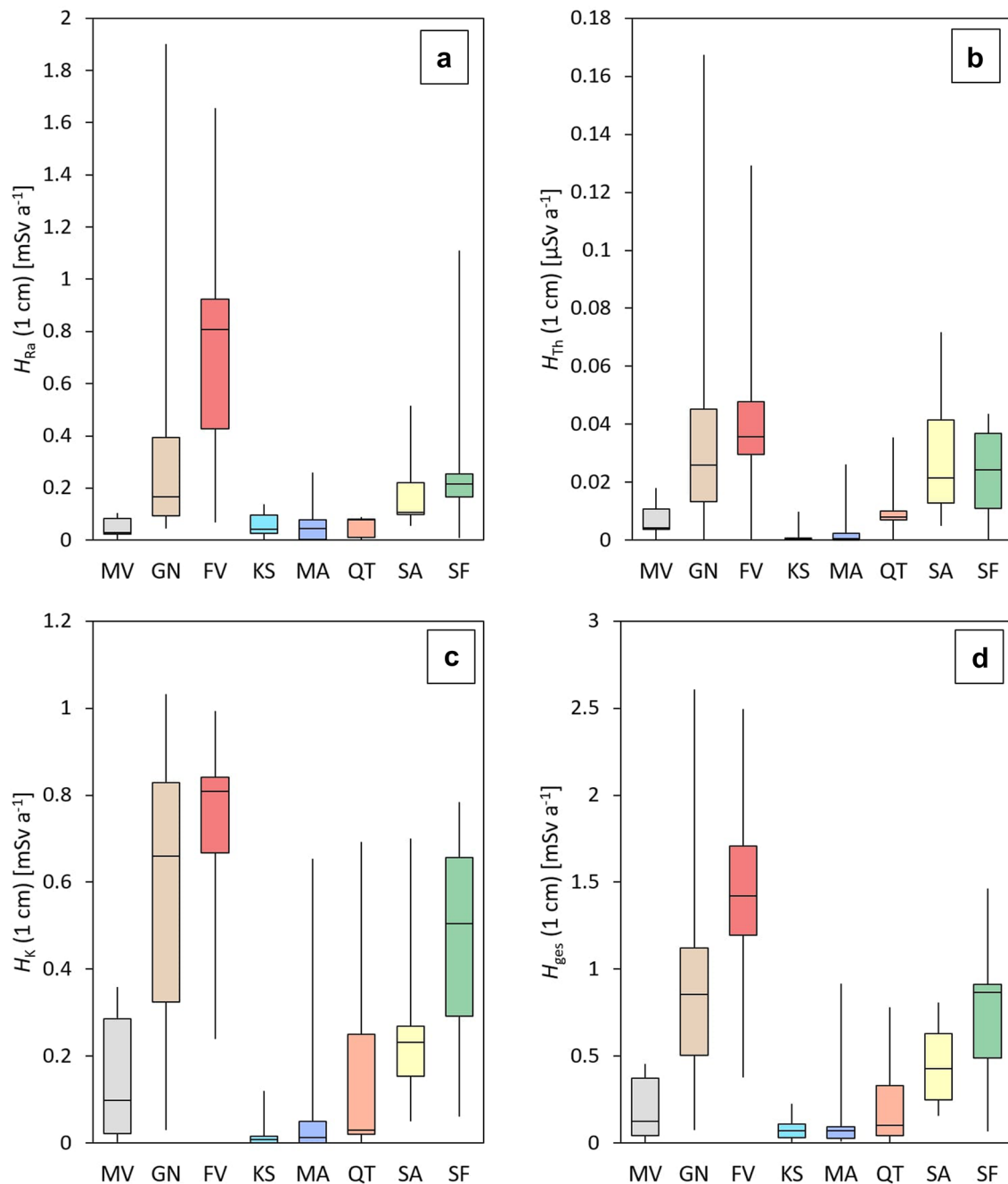


Fig. 5 The statistical summary of the lithological groups based on the equivalent doses H in mSv a^{-1} or $\mu\text{Sv a}^{-1}$ presented as boxplots; **a** for ^{226}Ra , **b** for ^{232}Th , **c** for ^{40}K and **d** for the total dose rate. The calcula-

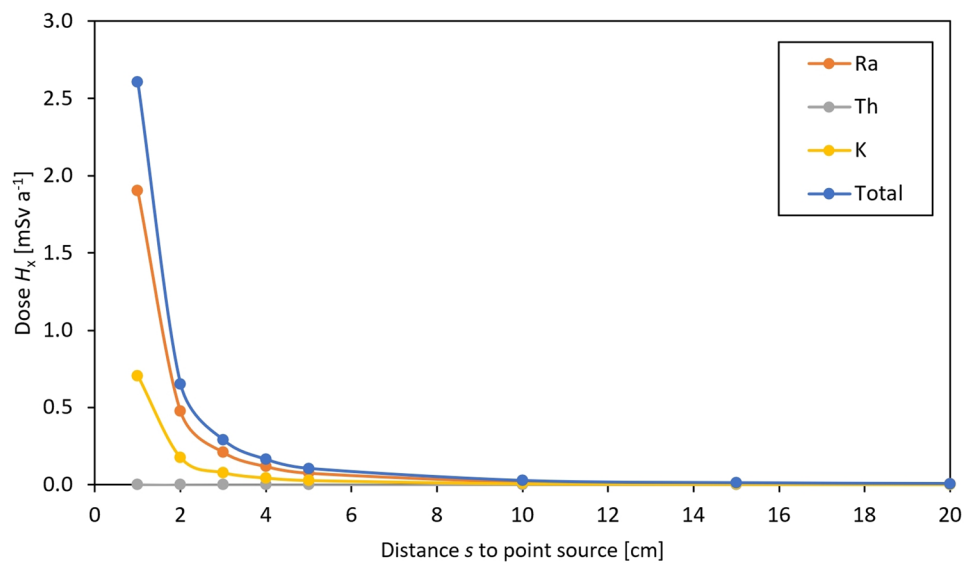
tion of the doses is assuming a distance $s=1$ cm to the radioactive source. The red line represents the legal upper limit of the dose rate ($H=1$ mSv a^{-1}) to which people may be exposed

granites in this project being 1003 Bq kg^{-1} . This comparison of the granites is shown in Table 3.

Gneisses have also been investigated for their radioactive properties in several studies. The gneisses from the literature have ^{226}Ra activities in the range of 9.70 Bq kg^{-1} and 352 Bq kg^{-1} , while the median for gneisses from this project is 17.78 Bq kg^{-1} . The activities of ^{232}Th from the literature

vary in the range of 8.94 – 100 Bq kg^{-1} , and the median for gneisses from this project is also 35.55 Bq kg^{-1} . The activities of ^{40}K of the gneisses from the literature ranged from 490 to 1569.46 Bq kg^{-1} , whereas the median of the gneiss analyses in this project is 738 Bq kg^{-1} . Marocchi et al. (2011) analysed the natural stone Kashmir White (Table 1). The measured values of this sample only partially agree

Fig. 6 Dependence of the dose H_x for ^{226}Ra , ^{232}Th , ^{40}K and the sum of the three nuclides with the distance to the point source for the gneiss sample Shiwakashi



with the literature data, especially large discrepancies are observed in the activities of ^{226}Ra and ^{40}K . The comparison of the gneisses is given in Table 4.

The rocks of the MV group given in Table 1 have generally not often been examined for their radiological character in the literature. The basalt Vietnam Black has significantly lower activities in all three measured nuclides than the other basalts from the literature. The Virginia Black sample has ^{232}Th activity in the same order of magnitude of the literature data, with ^{226}Ra activity slightly lower and ^{40}K activity far lower than is the case for the metagabbro samples from the literature. The trachyandesite from Armenia also has significantly lower activities in the three radionuclides than the literature data. The Verde Malenco sample has significantly lower activities in the measured radionuclides (all below the detection limit) than the other serpentine samples from the literature. The amphibolite sample, Via Lattea, has similar activities to the amphibolite analyses from the literature. For the comparison of the mafic rocks and their metamorphic products, see Table 5.

Sands and sandstones have often been studied radiologically in the literature, as they are the most common sediments on Earth. The activity of ^{226}Ra varies in the literature data between 3.1 and 104.23 Bq kg⁻¹, with a median of 16.37 Bq kg⁻¹ for the sandstones from this project. The activity of ^{232}Th is in the range of 3.7 Bq kg⁻¹ and 180.4 Bq kg⁻¹ in the literature data, whereas the median from this project is also 30.69 Bq kg⁻¹. ^{40}K has activities ranging from 39.82 to 1421 Bq kg⁻¹ in the literature data, with the median of the sandstones from this project being 305 Bq kg⁻¹. The comparison of the sandstones is shown in Table 6.

The pelitic rocks and their metamorphic products, schist and phyllite, have been studied for their radioactive characteristics in some papers. In the literature data, these rocks

have ^{226}Ra activities ranging from 7.52 to 68.2 Bq kg⁻¹ and the median for the clayey rocks from this project is 29.92 Bq kg⁻¹. The activities of ^{232}Th for these clayey rocks from the literature range from 31.74 and 65.3 Bq kg⁻¹, a range where the median from this project 37.89 Bq kg⁻¹ is included. The activities of ^{40}K vary in the literature data between 246.03 and 1016 Bq kg⁻¹, the median from this project is in this range with 592 Bq kg⁻¹. The comparison of these rocks is shown in Table 7.

Even if the limestones and travertines are not particularly dangerous radiologically, there is published work on their radioactive character. The activity of ^{226}Ra of limestones from the literature varies between 5 and 135.97 Bq kg⁻¹, whereas the median of the carbonates from this project is 8.04 Bq kg⁻¹. The ^{232}Th activities from the literature take values in the range of 3.1 Bq kg⁻¹ and 32.28 Bq kg⁻¹, whereas the median of the current project is somewhat lower at 0.90 Bq kg⁻¹. The activities of ^{40}K from the literature range from 20 to 251.31 Bq kg⁻¹, whereas the median from this project is also lower at 18.50 Bq kg⁻¹. The comparison of the carbonate rocks is shown in Table 8.

Besides limestone, quartzite is another lithology that has been studied less frequently due to its radiological insignificance. The activities of ^{226}Ra from the literature data vary between 6.94 and 77.5 Bq kg⁻¹, with the median from this project being 10.28 Bq kg⁻¹. The activity of ^{232}Th from the literature ranges from 6.3 to 10.54 Bq kg⁻¹ and the median from this project is 12.35 Bq kg⁻¹. The ^{40}K activities from the literature data take values from 140 to 226.4 Bq kg⁻¹, with the median from the current project being 165 Bq kg⁻¹. The comparison of the data from quartzite can be seen in Table 9.

Among “granites” in the international trade, the petrographic description is often not correctly denominated;

Table 3 Values for activities A for ^{226}Ra , ^{232}Th and ^{40}K from the literature for granites compared with the samples from this study

	A (^{226}Ra) [Bq kg $^{-1}$]	A (^{232}Th) [Bq kg $^{-1}$]	A (^{40}K) [Bq kg $^{-1}$]
Granite ^[1]	100	120	1000
Granite 1 ^[2]	64	68	1180
Granite 2 ^[2]	46	170	1155
Granite 3 ^[2]	48	315	1210
Granite ^[4]	133.31	147.12	1110.49
Granite ^[4]	50.41	82.25	1694.93
Granite ^[4]	122.31	104.17	2012.03
Granite ^[5]	57.4	53.4	1041.4
Granite ^[5]	39	47.9	1031
Granite ^[5]	76.1	70	1465.4
Rosa Porrino ^[8]	62	80	1160
Rosa sardo ^[8]	35	47	1030
Rosa Predazzo ^[8]	160	210	1230
Granite ^[10]	116	53	1290
Granite ^[13]	56.4	48.6	1492.8
Granite ^[13]	32.3	22.9	762.5
Granite ^[13]	10.1	80	1906
Granite ^[14]	92.71	29.19	1117.24
Granite ^[14]	40.39	91.55	1007.8
Azul noche ^[18]	59.7	50.8	954
Rubio Cardenosa ^[18]	39	11.7	1201
Silvestre Dorado ^[18]	118.4	53.3	1335
Los Santos ^[18]	75.5	71.9	1123
Gris Villa ^[18]	64.8	68.8	920
Sorihuela ^[18]	75.3	63.6	994
Granites ^[19]	45	39	1178
Median (FV)	105.35	50.67	1003

Values from the literature are marked with square brackets and references are listed at the end of the chapter. The median values of the samples (group FV) from this project are shown in bold. The literature data are taken from: Bundesamt für Strahlenschutz (2020), Deutscher Naturwerkstein-Verband (2019), Yalcin et al. (2020), Ahmed et al. (2006), Marocchi et al. (2011), Madruga et al. (2019), Mohamed et al. (2016), Rafique et al. (2014), Pereira et al. (2013), Zeghib et al. (2016), [1] Bundesamt für Strahlenschutz (2020), [2] Deutscher Naturwerkstein-Verband (2019), [3] Gehrcke et al. (2012), [4] Yalcin et al. (2020), [5] Ahmed et al. (2006), [6] Örgün et al. (2007), [7] El Aassy et al. (2011), [8] Marocchi et al. (2011), [9] Kovler et al. (2002), [10] Madruga et al. (2019), [11] Shohda et al. (2018), [12] Weng (1996), [13] Mohamed et al. (2016), [14] Rafique et al. (2014), [15] Turhan et al. (2009), [16] Aykamis and Kilic (2011), [17] Iqbal et al. (2000), [18] Pereira et al. (2013), [19] Zeghib et al. (2016)

therefore, sometimes marbles are also described as granitoides. Thus, radiological data of marbles can also be found in numerous works. The activities of ^{226}Ra from literature data vary from 2 to 95.17 Bq kg $^{-1}$, with the median from this project being 9.43 Bq kg $^{-1}$. The activities of ^{232}Th from the literature range from 0.1 to 110.73 Bq kg $^{-1}$, whereas the median from this project is 2.01 Bq kg $^{-1}$. The activities of ^{40}K in the literature range from 0.8 to 1054.65 Bq kg $^{-1}$, with the median from this project being 62.6 Bq kg $^{-1}$. The comparison of the marbles is shown in Table 10.

Model calculation of annual equivalent dose rates

The potential radiation exposure for humans can be calculate by very complex models (e.g. Markkanen 1995; Myatt et al. 2010). For this purpose, an array of different parameters is important and needs to be considered, such as the radiation activity of the natural stone used, the total volume of the installed stone, the cumulative daily and yearly duration of residence of a person in the observed room as well as their average distance to the walls (Zeghib et al. 2016).

To constrain our results in the context of everyday life, the potential annual equivalent doses were calculated using two extreme, hypothetical approaches. The first model, “Small room”, describes a square room, where the floor, ceiling and

Table 4 Values for activities A for ²²⁶Ra, ²³²Th and ⁴⁰K from the literature for gneisses compared with the samples from this project

	A(²²⁶ Ra) [Bq kg ⁻¹]	A(²³² Th) [Bq kg ⁻¹]	A(⁴⁰ K) [Bq kg ⁻¹]
Gneiss ^[1]	75	43	900
Gneiss ^[2]	75	43	900
Metagranite ^[3]	9.70	30.97	623.95
Metagranite ^[3]	50.75	79.35	1569.46
Kashmir white ^[8]	352	33	1100
Beola Valdossola ^[8]	14	24	490
Serizzo Valdossola ^[8]	48	40	740
Pietra Luserna ^[8]	115	100	1050
Gneiss ^[14]	108.54	24.79	1135.55
Gneiss ^[14]	15.14	8.94	53.44
Gneiss Zamora ^[18]	77.6	68.8	1421
Kashmir White	16.995	30.84	420.8
Median (GN)	17.78	35.55	738

Values from the literature are marked with square brackets and references are listed at the end of the chapter. The median values of the GN samples (group GN) and our data on Kashmir White are shown in bold. The literature data refer to: Bundesamt für Strahlenschutz (2020), Deutscher Naturwerkstein-Verband (2019), Gehrcke et al. (2012), Marocchi et al. (2011), Rafique et al. (2014), Pereira et al. (2013)

walls are covered by 3-cm-thick stone tiles. The dimensions of the room are 2 × 2 × 2 m and there are no further objects (doors, windows etc.) inside the room. It is assumed that the room is completely shielded from the external radiation; therefore, the effects of the background radiation (cosmic and terrestrial radiation) are not considered. The radioactive dose for the centre of the room is calculated. Since the origin of the measured activities are point sources, it is necessary to alternatively recalculate the activities for a surface. Therefore, a volume of 1 cm³ is assumed for each single point source. In such a manner, a total of 40,000 point sources are quantified for the total of a 6 × 4 m² (24m²) wall surface area for each side with the thickness of 1 cm. Subsequently, there are three 1-cm-thick “layers” defined from the assumed total tile thickness of 3 cm. So the total amount of point sources adds up to 120,000 for the wall in total. Since the two rear layers are covered by the layers of point sources in front of them, an effect of attenuation is generated for the reference point in the middle of the room. To calculate this effect of attenuation, a shielding calculator from the DAMP engineering office (Ingenieurbüro DAMP) was used to determine the attenuation factors (SF) for the rear (SF₃) and the middle layer (SF₂) in the wall; it is not necessary for the front layer (SF₁), as there is no shielding material between it and the reference point. From the selection of materials for the calculator, normal concrete was chosen as shielding material, since it best represents the shielding parameters of the

Table 5 Values for activities A for ²²⁶Ra, ²³²Th and ⁴⁰K from the literature for samples of mafic rocks or their metamorphic products compared with the samples from this project

	A(²²⁶ Ra) [Bq kg ⁻¹]	A(²³² Th) [Bq kg ⁻¹]	A(⁴⁰ K) [Bq kg ⁻¹]
Basalt ^[1]	26	29	270
Basalt ^[9]	12	13.7	308.5
Basalt ^[12]		20	416
Vietnam Black	3.932	6.275	125
Metagabbro ^[5]	19.9	13.3	593.2
Metagabbro ^[5]	9.4	5.6	239.8
Metagabbro ^[5]	15.2	6.4	176.5
Virginia Black	2.35	4.42	9.42
Tufo Grigio Riano ^[8]	137	290	1770
Peperino Viterbese ^[8]	100	140	1210
Trachy andesit armenien	16.24	24.26	563
Serpentinite ^[5]	22.5	17.2	481.6
Serpentinite ^[5]	6.2	6	84.5
Serpentinite ^[5]	5.7	3.4	10.9
Serpentinite ^[11]	16.11	20.74	309.01
V. Malenko	< 0.6634	< 1.433	< 2.321
Amphibolite ^[5]	10.4	4.8	197.7
Amphibolite ^[5]	5.1	3.9	10.8
Via Lattea	2.91	4.705	36.9

The values from the literature are marked with square brackets and the references are listed at the end of the chapter. The values of the corresponding MV samples from Table 1 are shown in bold. The literature data refer to: Bundesamt für Strahlenschutz (2020), Ahmed et al. (2006), Marocchi et al. (2011), Kovler et al. (2002), Shohda et al. (2018), Weng (1996)

natural stones. Since each radionuclide has a characteristic equivalent dose rate constant Γ_H [nSv qm h⁻¹ GBq⁻¹], they also possess distinct attenuation factors (Table 11). The following equation (Eq. 4):

$$H = \frac{\Gamma_H \cdot A}{r^2} \tag{4}$$

is applied as a basis for the calculation of the equivalent dose rate H [μSv h⁻¹], where A is the activity of the respective nuclides (²²⁶Ra, ²³²Th, ⁴⁰K) in GBq and r is the distance from the radiation source in metre (m) using the inverse-square law. For the assumed case that a 2-m-tall person is in the centre of the room, the average distance of the wall surfaces to the centre of the room is calculated with the equation:

$$r = \frac{1 \cdot r_{\min} + 2 \cdot r_{\max}}{3} \tag{5}$$

Table 6 Values for activities A for ^{226}Ra , ^{232}Th and ^{40}K in Bq kg $^{-1}$ from the literature for sand and sandstone samples compared with the samples from this project

	$A(^{226}\text{Ra})$ [Bq kg $^{-1}$]	$A(^{232}\text{Th})$ [Bq kg $^{-1}$]	$A(^{40}\text{K})$ [Bq kg $^{-1}$]
Sand ^[1]	15	16	380
Beach sand ^[6]		96.6	1421
Beach sand ^[6]		180.4	862.8
Beach sand ^[6]		149.4	1389.2
Sandstone ^[7]	67.82	45.36	39.82
Sandstone ^[7]	50.88	15	161.19
Sandstone ^[7]	104.23	27.62	52.66
Sand ^[9]	3.1	3.7	90.9
Sandstone ^[12]		50	539
Sandstone ^[14]	45.19	68.89	449.22
Sandstone ^[14]	40.68	64.45	609.93
Sandstone ^[14]	41.4	65.49	439.48
Arenisca Quintanar ^[18]	21.3	7.8	485
Quintanar Beige ^[18]	9	9.1	332
Rojo San Adrian ^[18]	27.1	25.2	749
Sierra Demanda ^[18]	22.6	6	410
Zamora ^[18]	23.4	23.7	439
Median (SA)	16.37	30.69	305

The values from the literature are marked with square brackets and the references are listed at the end of the chapter. The median values of the samples (group SA) are shown in bold. The literature data refer to: Bundesamt für Strahlenschutz (2020), Örgün et al. (2007), El Aassy et al. (2011), Weng (1996), Rafique et al. (2014), Pereira et al. (2013)

$$H = \frac{\frac{A_X \cdot \Gamma_{HX}}{r^2 \cdot SF_1} \cdot 40000 + \frac{A_X \cdot \Gamma_{HX}}{r^2 \cdot SF_2} \cdot 40000 + \frac{A_X \cdot \Gamma_{HX}}{r^2 \cdot SF_3} \cdot 40000}{V_B} \quad (6)$$

For the application of this model, Eq. (5) was modified to Eq. (6).

Hence, the equivalent dose rate H is calculated in three separate terms, as different attenuation factors are effective for each respective cladding with the tiles. The summed up terms are divided by the volume of the sample box (V_B), as the activity units are given in GBq kg $^{-1}$ rather than in Bq per sample. The certified volume of 250 ml for the vessels is referred to a normal fill level. A volume of 280 ml was adopted for the calculations, since the sample boxes were completely filled. The volume of 280 ml was estimated by filling a single sample box with water. Additionally, the calculated equivalent dose rate is multiplied by the number of walls and the units are converted from nSv h $^{-1}$ to mSv a $^{-1}$.

For the second model, “Coffin”, Eq. 5 was adjusted to room dimensions of 1.8 × 0.8 × 0.4 m. Thereby, two surfaces with 1.44 m 2 , two with 0.72 m 2 and two with 0.32 m 2 . The average distances to the centre of the room of 0.73 m (r_{\min}),

Table 7 Values for activities A for ^{226}Ra , ^{232}Th and ^{40}K in Bq from the literature for samples of the claystones and their metamorphic products compared with the samples from this project

	$A(^{226}\text{Ra})$ [Bq kg $^{-1}$]	$A(^{232}\text{Th})$ [Bq kg $^{-1}$]	$A(^{40}\text{K})$ [Bq kg $^{-1}$]
Clay ^[1]	<40	60	1000
Clay ^[1]	40		560
Beola Dorata ^[8]	18	58	740
Slate ^[10]	31	56	829
Shale ^[12]		51	813
Schist ^[14]	35.52	55.6	437.61
Shale ^[14]	20.83	33.98	246.03
Shale ^[14]	32.05	54.97	537.5
Shale ^[14]	68.2	35.94	381.33
Slate ^[14]	37.28	65.01	879.78
Shale ^[14]	7.52	31.74	428.66
Filita Bernardos ^[18]	55.7	65.3	1016
Median (SF)	29.92	37.89	592

The values from the literature are marked with square brackets and the references are listed at the end of the chapter. The median value of the SF samples is given in bold. The literature data refer to: Bundesamt für Strahlenschutz (2020), Marocchi et al. (2011), Madruga et al. (2019), Weng (1996), Rafique et al. (2014), Pereira et al. (2013)

Table 8 Values for activities A for ^{226}Ra , ^{232}Th and ^{40}K from the literature for limestones and related rocks compared with the samples from this project

	$A(^{226}\text{Ra})$ [Bq kg $^{-1}$]	$A(^{232}\text{Th})$ [Bq kg $^{-1}$]	$A(^{40}\text{K})$ [Bq kg $^{-1}$]
Calcareous Sandstone ^[1]	15	10	200
Travertine ^[2]	5	5	20
Calcareous Sandstone ^[3]	10		130
Dolostone ^[7]	135.97	3.41	17.59
Dolomite ^[9]	28	3.1	33.6
Limestone ^[9]	18.3	7.4	77.1
Limestone ^[12]		5.1	80
Limestone ^[14]	18.06	28.73	224.14
Limestone ^[14]	25.38	32.38	251.31
Limestone ^[14]	23.19	31.66	236.71
Median (KS)	8.04	0.90	18.5

The values from the literature are marked with square brackets and the references are listed at the end of the chapter. The median value of the samples (group KS) referring to Table 1 is shown in bold. The literature data refer to: Bundesamt für Strahlenschutz (2020), Deutscher Naturwerkstein-Verband (2019), Gehrecke et al. (2012), El Aassy et al. (2011), Kovler et al. (2002), Weng (1996), Rafique et al. (2014)

0.8 m and 0.97 m (r_{\max}), respectively, were assumed. The background radiation was neglected in this model as well.

The calculated annual dose rates for the models 1 and 2 are displayed in Fig. 5. The activity values of at least

Table 9 Values for activities A for ²²⁶Ra, ²³²Th and ⁴⁰K in Bq kg⁻¹ from the literature for quartzites compared with the samples from this project

	A(²²⁶ Ra) [Bq kg ⁻¹]	A(²³² Th) [Bq kg ⁻¹]	A(⁴⁰ K) [Bq kg ⁻¹]
Marble ^[10]	6.1	1.9	34
Marble ^[11]	27.01	9.03	103.56
Marble ^[11]	14.63	9.41	81.24
Marble ^[11]	15.04	6.88	168.26
Marble ^[13]	5.7	0.1	0.9
Marble ^[13]	7.3	0.9	0.96
Marble ^[13]	2	0.31	0.8
Marble ^[14]	22.48	2.22	15.67
Marble ^[14]	5.35	< 1.80	9.55
Marble ^[14]	95.17	9.72	655.73
Marble ^[14]	54.14	110.73	1054.65
Marble ^[14]	40.55	64.03	812.16
Marble ^[17]	33	32	57
Median (MA)	9.43	2.01	62.6

Values from the literature are marked with square brackets and references are listed at the end of the chapter. The median value of the samples (group QT) from this paper is shown in bold. The literature data refer to Turhan et al. (2009) and Aykamis and Kilic (2011)

Table 10 Values for activities A for ²²⁶Ra, ²³²Th and ⁴⁰K from the literature for marbles compared with the samples from this project

	A(²²⁶ Ra) [Bq kg ⁻¹]	A(²³² Th) [Bq kg ⁻¹]	A(⁴⁰ K) [Bq kg ⁻¹]
Quartzite ^[15]	77.5	6.3	140
Quartzite ^[16]	6.94	7.34	140.05
Quartzite ^[16]	9.85	10.54	226.4
Median (QT)	10.28	12.35	165

The values from the literature are marked with square brackets and the references are listed at the end of the chapter. The median value of the samples (group MA) from this project is shown in bold. The literature data refer to: Madruga et al. (2019), Shohda et al. (2018), Mohamed et al. (2016), Rafique et al. (2014), Iqbal et al. (2000)

one of the measured radionuclides laid below the limit of detection for the total of 15 out of 82 investigated samples. For the affected nuclides in these samples, an activity of A = 0 Bq was set for the further calculations. The calculated equivalent dose rates from the model 1 vary from <0.01 to 0.79 mSv a⁻¹ (for the sample *Giallo California*). Thus, no measured sample exceeds the annual dose rate of 1 mSv a⁻¹, which is set as the maximal value for the German regulations. The annual dose rate for a total of 24 samples was calculated to be in the critical region of 0.3 to 1 mSv a⁻¹ and should therefore not be installed as stone tiles prior to further investigations. It is noticeable that the annual dose rates calculated based on the model 2 are significantly higher

Table 11 Listed are the equivalent dose rate constant Γ_H in mSv qm h⁻¹ Bq⁻¹, taken from the shielding calculator of DAMP, and the attenuation factor for the wall thicknesses/shielding thicknesses: 0, 10 and 20 mm for the respective radionuclides ²²⁶Ra, ²³²Th and ⁴⁰K

	²²⁶ Ra+	²³² Th+	⁴⁰ K
Equivalent dose constant Γ _H [mSv qm h ⁻¹ Bq ⁻¹]	0.000298	0.000193	0.0000211
Attenuation coefficient			
0 mm	1	1	1
10 mm	1	1	1.03
20 mm	1.02	1.03	1.06

They were determined with the help of the shielding calculator of DAMP Ingenieurbüro (Ingenieurbüro DAMP 2020)

than for the model 1. For the model 2, the annual dose rates vary between <0.01 and 1.29 mSv a⁻¹, calculated for the sample *Giallo California*. An annual dose rate exceeding the limit of 1 mSv a⁻¹ was calculated for a total of 16 samples, whereas for another 34 samples the determined annual dose rate was in the critical area of 0.3–1 mSv a⁻¹. The higher annual dose rates from the second model are derived from the smaller distance of the radioactive sources to the centre of the room (inverse-square law), as the goal of this model was to enclose a person as close as possible with stone tiles from all sides. Even though the approach “what equivalent dose rate affects a person when enclosed in a coffin for a year” is not entirely realistic, it is shown that even when enclosed with material with the highest dose rate values (here *Giallo California*) of 1.29 mSv a⁻¹, a dose far below the maximum dose of 20 mSv a⁻¹ is experienced, which is set for people with occupational radiation exposure in Germany (Bundesamt für Strahlenschutz 2020).

Model calculation of radon exposure

The contribution of the building materials to the indoor radon can be simulated on the basis of the data obtained for the exhalation rate of the same materials. For this goal, the radon concentration (C_{Rn}) can be calculated from the following equation (Eq. 7) taken also in account the ventilation rate:

$$C_{Rn} = E_m * M / (\lambda o + \lambda v) * V \tag{7}$$

were E_m is the exhalation rate by mass (in Bq kg⁻¹ h⁻¹), M is the mass of the stone used as building material (in kg), λo is the radon decay rate (0.0076 h⁻¹), λv is the ventilation rate (in h⁻¹), and V is the volume of the room (in m³). M is the product of the density of the material by the volume of the tiles used. The product of E_m * M is designated also as the radon entry (in Bq h⁻¹).

The radon concentration is calculated for a room with the dimensions of $4 \times 3 \times 2.5$ m, including a window of 1×1 m and a door with 2×1 m. Tiles of stone materials with different thickness (variable between 0.01 and 0.2 m) cover all the walls and the floor (Fig. 7). It is assumed no other contribution to indoor radon beside the stone material. Different ventilation rates is allowed and tested, assuming a value of $\lambda v = 0.2 \text{ h}^{-1}$ as representative of a poorly ventilated room and 0.5 h^{-1} as of the opposite case.

The results related to the worst situation in what concern to radon exposure in the room, considering a low ventilation rate, is shown in Fig. 8 for the different lithological groups. In the first case (tiles with a thickness of 1 cm), all the stone materials comply with the european legislation, with modelled maximum indoor radon less than 100 Bq m^{-3} . For tiles with thickness of 3 cm the same scenario is forecasted, despite the general increase in the radon concentrations; the highest averages are related with the FV group (granites), followed by the gneisses (GN group).

For higher tiles thickness, and for poorly ventilated spaces, some of the building materials can induce indoor radon concentrations above the action limit, as expected all included in the FV group (Fig. 7). This is the case of the Waldstein, the Flossenburger, the Amarelo Real, for 10-cm-thick tiles, but for higher thickness (20 cm) others show the same behaviour, as the case of the Coral Red and, in less extend, the Branco Micaela and the Kuperscheifer types; this last rock is the only one not included in the FV group (SF).

The ventilation is a crucial parameter to control the indoor radon concentrations, as expected, and for higher rates ($\lambda v = 0.5 \text{ h}^{-1}$) only the more problematic rocks (Waldstein, the Flossenburger, the Amarelo Real) are able to increase the indoor radon concentrations up to the action limit (Fig. 8).

Final remarks

Natural stones are widely used as construction material both in outdoor and indoor applications. Their optical and physico-mechanical properties, together with the distribution and availability make them an excellent construction material. In the last decades, the potential radioactivity harmful of the materials has been discussed in scientific papers and several laws and recommendations were published regarding this concern. In line of this, the European Union published some principles for limiting the natural radioactivity of building materials. The future of this important economic activity needs to incorporate these new principles and a deep evaluation of building stones will be necessary to avoid or limit any eventual constraints to the utilization of the rocks as construction materials.

In the near future, global market will demand the assessment of the radiological hazards of thousands of building

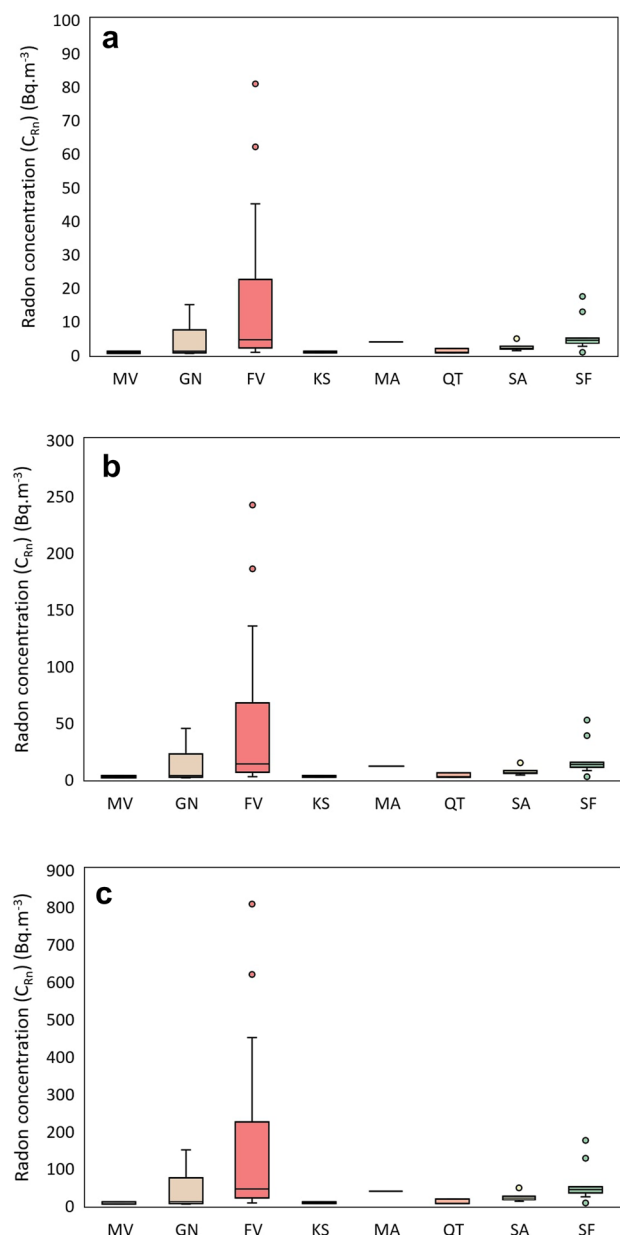


Fig. 7 Indoor radon concentrations calculated from the model discussed in the text, considering a low ventilation rate scenario and different thickness of the tiles (from above: 1 cm, 3 cm and 10 cm)

stones produced worldwide. This research is a first step to have a general overview of this problematic. A wide range of samples were selected regarding the mineralogy and the geological background. Eighty-two rocks were selected to measure their radioactivity and calculate the resulting annual equivalent doses and radon exhalation. The samples with similar petrographical characteristics were grouped resulting into eight different groups: mafic, gneisses, felsic, limestones, marbles, quartzite, sandstones and similar sedimentary rocks and metamorphic rocks.

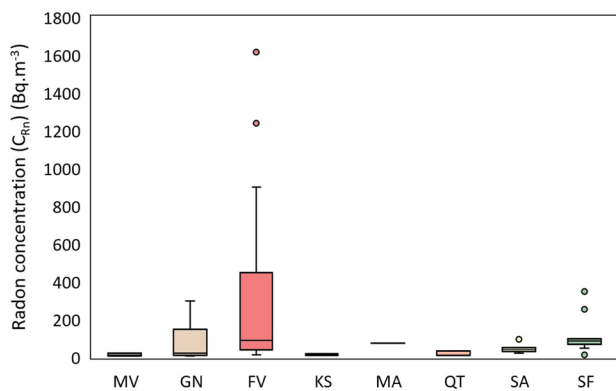


Fig. 8 Indoor radon concentrations calculated from the model discussed in the text, considering a high ventilation rate scenario and 20-cm-thick tiles

The activity concentration of radon, thorium and potassium, $A^{226}\text{Ra}$, $A^{232}\text{Th}$ and $A^{40}\text{K}$, for most of the samples is below the upper limits of normal activities ($A^{226}\text{Ra}$ and $A^{232}\text{Th} < 100 \text{ Bq kg}^{-1}$ and $A^{40}\text{K} < 1000 \text{ Bq kg}^{-1}$) for construction materials (European Commission 1999). However, differences are evident among the several rock groups. Mineralogy and geological process have a great influence on the isotope content. A clear contrast is seen between the felsic (high values) and mafic rocks (low values) in terms of Ra activity as consequence of the incorporation of uranium and thorium in the crystal lattices of the minerals. Marble and limestone show low activities values, despite some conditions to high uranium concentrations can be found. In the sandstones and other sedimentary rocks, the source of the sediments plays an important role in their chemical and mineralogical composition. In these rocks, elevated uranium and thorium contents may be caused by a greater amount of heavy minerals originate from a felsic magmatic source area. Similarly to the sandstones, low concentrations of uranium and thorium are usually expected in the quartzite group. The metamorphic rocks, as slates and phyllites, show a very high variance of the activities of radium and potassium.

Clay minerals have the ability to incorporate uranium in different ways specially in sedimentary layers with a high organic content. The metamorphic products of the mudstones, shales and phyllites, are largely composed of different clay minerals, such as illite, vermiculite and chlorite, which may contain high levels of potassium. The gneisses show the broadest spectrum of isotopes activities, because they can form as a metamorphic product of many different rocks under diverse P–T conditions. Therefore, the concentrations of uranium, thorium and potassium in the gneiss samples are very dependent on the source rock.

The activity indices (I) were assessed in the case of exaggerated thickness ($d=20 \text{ cm}$). Samples of gneiss, felsic and metamorphic groups rock groups have activity indices mainly in the range $0.5 \leq I \leq 1$, with individual samples having higher indices up to $I=1.87$. The other rock groups are clearly below $I=0.5$, and only some samples exceed this value. Since the natural stones are used indoors as thinner cover slabs, lower activity indices are to be expected in reality and none further investigations are needed.

The felsic rocks present the highest median exhalation rates for both ^{222}Rn and ^{220}Rn , followed by metamorphic rocks such as slates, phyllites and metapelites, while the lowest exhalation rates are observed in mafic rocks, limestones and travertines.

According to the principles of radiological safety, all building materials that produce a dose of $H > 1 \text{ mSv a}^{-1}$ may only be used in special cases (European Commission 1999). Assuming an exposure time of 8760 h (corresponding to a whole year) and a distance to the source of only 1 cm, a total of 24 samples show a critical dose of $H > 1 \text{ mSv a}^{-1}$ (values between 0 and 2.61 mSv a^{-1}). Since no person is in this proximity to the slabs and tiles throughout all the year, and considering that the equivalent dose decreases in a quadratic relation to the distance, the radiation from these samples poses no danger and they may be used legally without restrictions.

In some cases, like a small and poorly ventilated room covered by tiles, the modelling of the annual equivalent dose rates and radon exposure can reach the maximum values. The values obtained characterize unrealistic cases and allow to have an idea about the possible harm of the building material.

Unfortunately, this topic is not yet a cause of concern for most of the producers. Considering the new insights and the regulations, developments are expected in a near future. This research rather than evaluate the radiological hazards of all the building materials, a task for several decades, intends to highlight the main factors regarding this topic. Both consumers, producers and market organizations should be aware of this new challenge.

Acknowledgements This study was supported by the Fundação para a Ciência e a Tecnologia in the frame of the UIDB/00073/2020 and UIDP/00073/2020 projects of the I&D unit Geosciences Center (CGEO). We are also very grateful by the help of Marvin Blaue during the measurements and Karl-Jochen Stein with the rock sampling.

Funding Open Access funding enabled and organized by Project DEAL.

Declarations

Conflict of interest The authors declare that there are no conflict of interest.

Open Access This article is licensed under a Creative Commons Attribution 4.0 International License, which permits use, sharing, adaptation, distribution and reproduction in any medium or format, as long as you give appropriate credit to the original author(s) and the source, provide a link to the Creative Commons licence, and indicate if changes were made. The images or other third party material in this article are included in the article's Creative Commons licence, unless indicated otherwise in a credit line to the material. If material is not included in the article's Creative Commons licence and your intended use is not permitted by statutory regulation or exceeds the permitted use, you will need to obtain permission directly from the copyright holder. To view a copy of this licence, visit <http://creativecommons.org/licenses/by/4.0/>.

References

- Ahmed NK, Abbadly A, El Arabi AM, Michel R, El-Kamel AH, Abbadly AGE (2006) Comparative study of the natural radioactivity of some selected rocks from Egypt and Germany. *Indian J Pure Appl Phys* 44(3):209–215
- Al-Hamarneh IF (2017) Radiological hazards for marble, granite and ceramic tiles used in buildings in Riyadh, Saudi Arabia. *Environ Earth Sci* 76:516. <https://doi.org/10.1007/s12665-017-6849-5>
- Allen JG, MacIntosh DL, Minegishi SJH, Mccarthy JF (2013) Predicted indoor radon concentrations from a Monte Carlo simulation of 1 000 000 granite countertop purchases. *J Radiol Prot* 33:151–162. <https://doi.org/10.1088/0952-4746/33/1/151>
- Ames LL, McGarrah JE, Walker BA (1983) Sorption of uranium and radium by biotite, muscovite, and phlogopite. *Clays Clay Miner* 31(5):343–351
- Anjos RM, Ayub J, Cid AS, Cardoso R, Lacerda T (2011) External gamma-ray dose rate and radon concentration in indoor environments covered with Brazilian granites. *J Environ Radioact* 102:1055–1061
- Aykamis AS, Kilic AM (2011) Natural radionuclide distribution in quartzite sands of East Mediterranean Region (Turkey). *Bull Eng Geol Env* 70(2):317–321
- Bayer G, Rogers JJW, Adams JAS, Haack UK (1969) Thorium. *Handbook of geochemistry*. Springer
- Bone SE, Dynes JJ, Cliff J, Bargar JR (2017) Uranium(IV) adsorption by natural organic matter in anoxic sediments. *Proc Natl Acad Sci* 114(4):711–716
- Broecker WS, Li YH, Cromwell J (1967) Radium-226 and radon-222: concentration in Atlantic and Pacific Oceans. *Science* 158(3806):1307–1310
- Bundesamt für Strahlenschutz (2020) Natürliche Radionuklide in Baumaterialien. Radioaktivität in Der Umwelt. https://www.bfs.de/DE/themen/ion/umwelt/baustoffe/radionuklide/radionuklide_node.html
- Burch PRJ (1953) Specific γ -activity, the branching ratio and half-life of potassium-40. *Nature* 172(4373):361–362
- Burkin W, Villert J (2017) Simultaneous Radon/Thoron discrimination using the AlphaGuard. Bertin Instruments. RADN-300-DE001, 22/02.
- Cecil LD, Green JR (2000) Radon-222. *Environmental tracers in subsurface hydrology*. Springer, pp 175–194
- Chikkur GC, Umakantha N (1977) Half-life of thorium-232: a laboratory experiment. *Am J Phys* 45(11):1120–1122
- Cumberland SA, Douglas G, Grice K, Moreau JW (2016) Uranium mobility in organic matter-rich sediments: a review of geological and geochemical processes. *Earth Sci Rev* 159:160–185
- De With G, Michalik B, Hoffmann B, Döse M (2018) Development of a European harmonised standard to determine the natural radioactivity concentrations in building materials. *Constr Build Mater* 171:913–918
- Deutscher Naturwerkstein-Verband (2019) Strahlung natürlicher Baustoffe. https://www.natursteinverband.de/fileadmin/redaktion/downloads/Fachinformation_PDF/DNV-Info-Strahlung_2019.pdf. 1–2
- DIN 11929 (2020) Bestimmung der charakteristischen Grenzen (Erkennungsgrenze, Nachweisgrenze und Grenzen des Überdeckungsintervalls) bei Messungen ionisierender Strahlung - Grundlagen und Anwendungen - Teil 1: Elementare Anwendungen (ISO 11929-1:2019). Beuth Verlag, Berlin, p 51
- Domingos F, Pereira A (2018) Implications of alteration processes on radon emanation, radon production rate and W-Sn exploration in the Panasqueira ore district. *Sci Total Environ* 622–623:825–840. <https://doi.org/10.1016/j.scitotenv.2017.12.028>
- Domingos FP, Sêco SL, Pereira AJ (2021) Thoron and radon exhalation and emanation from granitic rocks outcropping in the Central Iberian Zone (Portugal). *Environ Earth Sci* 80(22):1–18
- Dostal J, Capedri S (1978) Uranium in metamorphic rocks. *Contrib Miner Petrol* 66(4):409–414
- El Aassy IE, El Galy MM, Nada AA, El Feky MG, Abd El Maksoud TM, Talaat SM, Ibrahim EM (2011) Effect of alteration processes on the distribution of radionuclides in uraniumiferous sedimentary rocks and their environmental impact, southwestern Sinai, Egypt. *J Radioanal Nuclear Chem* 289(1):173–184
- El-Gamal H, Sidique E, El-Haddad M, Farid ME (2018) Assessment of the natural radioactivity and radiological hazards in granites of Mueilha area (South Eastern Desert, Egypt). *Environ Earth Sci* 77:691. <https://doi.org/10.1007/s12665-018-7880-x>
- European Commission (1999) Radiological protection principles concerning the natural radioactivity of building materials - Radiation Protection 112 European Commission 1–16. <https://ec.europa.eu/energy/sites/ener/files/documents/112.pdf>
- Frondel JW, Fleischer M (1952) A Glossary of uranium- and thorium-bearing minerals, 2nd edn. United States Department of the Interior
- Fuller AJ, Leary P, Gray ND, Davies HS, Mosselmans JFW, Cox F, Robinson CH, Pittman JK, McCann CM, Muir M, Graham MC, Utsunomiya S, Bower WR, Morris K, Shaw S, Bots P, Livens FR, Law GTW (2020) Organic complexation of U(VI) in reducing soils at a natural analogue site: implications for uranium transport. *Chemosphere* 254:126859
- García-Talavera M, García-Pérez A, Rey C, Ramos L (2013) Mapping radon-prone areas using radiation dose rate and geological information. *J Radiol Prot* 33:605–620. <https://doi.org/10.1088/0952-4746/33/3/605>
- Gehrcke K, Hoffmann B, Schkade U, Schmidt V, Wichterle K (2012) Natürliche Radioaktivität in Baumaterialien und die daraus resultierende Strahlenexposition. https://doris.bfs.de/jspui/bitstream/urn:nbn:de:0221-201210099810/3/BfS_2012_SW_14_12.pdf
- Goswami S, Kumar Upadhyay P, Saravanan B, Natarajan V, Babu Verma M (2019) Two types of uranium mineralization in Gulcheru quartzite: fracture-controlled in Ambakapalle area and litho-controlled in Tummalapalle area, Cuddapah Basin, Andhra Pradesh, India. *China Geol* 2(2):142–156
- Guillén J, Tejado JJ, Baeza A, Corbacho JA, Muñoz JG (2018) Assessment of radiological hazard of commercial granites from Extremadura (Spain). *J Environ Radioact* 132:81–88. <https://doi.org/10.1016/j.jenvrad.2014.02.004>
- Hamdy MM, Aly GA (2011) Preliminary results of a first record of gold and uranium in marble from Central Eastern Desert, Egypt: a witness for (syn- and post-?) metamorphic mineralization in metasediments. *Arab J Geosci* 4(1–2):25–43
- Heier KS, Rhodes JM (1966) Thorium, uranium and potassium concentrations in granites and gneisses of the Rum Jungle complex, Northern Territory, Australia. *Econ Geol* 61(3):563–571

- Hidaka H, Horie K, Gauthier-Lafaye F (2007) Transport and selective uptake of radium into natural clay minerals. *Earth Planet Sci Lett* 264(1–2):167–176
- IAEA (2014) The Environmental Behaviour of Radium: Revised Edition. Technical Reports 476. <https://www.iaea.org/publications/10478/the-environmental-behaviour-of-radium-revised-edition>
- IAEA (1989) Uranium deposits in magmatic and metamorphic rocks. International Atomic Energy Agency
- IAEA (2014) The environmental behaviour of radium: revised edition. Technical Reports, 476
- Ingenieurbüro DAMP Abschirmrechner. Strahlenschutz Im Medizinischen Bereich. Retrieved 4 Dec 2020. from <http://strlrsch.de/abschirmrechner.html>
- Inoue A (1983) Potassium fixation by clay minerals during hydrothermal treatment. *Clays Clay Miner* 31(2):81–91
- Iqbal M, Tufail M, Mirza SM (2000) Measurement of natural radioactivity in marble found in Pakistan using a NaI(Tl) gamma-ray spectrometer. *J Environ Radioact* 51(2):255–265
- Ishikawa M, Ichikuni M (1984) Uptake of sodium and potassium by calcite. *Chem Geol* 42(1–4):137–146
- Jain AK (1972) Heavy Minerals in Precambrian Quartzite of the Lesser Himalaya, Garhwal, India. *SEPM J Sediment Res* 42(4):941–960
- Joel ES, Maxwell O, Adewoyin OO, Ehi-Eromosele CO, Saeed MA (2018) Comparative analysis of natural radioactivity content in tiles made in Nigeria and imported tiles from China. *Sci Rep* 8(1):1842
- Khan MS (2014) Azam A (2014) Measurements of indoor radon, thoron, and their progeny using twin cup dosimeters in rural areas of Northern India. *Environ Earth Sci* 71:1319–1325. <https://doi.org/10.1007/s12665-013-2538-1>
- Klepper MR, Wyant DG (1957) Notes on the geology of uranium. *Geol Surv Bull* 1046-F, 148
- Klinkhammer G, Palmer M (1991) Uranium in the oceans: where it goes and why. *Geochim Cosmochim Acta* 55(7):1799–1806
- Kovler K, Haquin G, Manasherov V, Nee'man E, Lavi N (2002) Natural radionuclides in building materials available in Israel. *Build Environ* 37(5):531–537
- Larsen E, Gottfried D (1960) Uranium and thorium in selected suites of igneous rocks. *Am J Sci (U.S.)* 258-A, 151–169
- Lide DR (2008). In: Lide DR (ed) CRC handbook of chemistry and physics, 89th edn. CRC Press
- Lindeman C, Oglesbee T, McLeod C, Krekeler MPS (2020) Mineralogy and geochemistry of the Kinnikinic Quartzite at the Arco Hills Silica and Gold Project in Butte County, Idaho: results of an ore quality spot check and implications for potential plasma furnace processing. *Minerals* 10(6):523
- Lyngkhai B, Nongkynrih P (2020) Radioactivity in building materials and assessment of risk of human exposure in the East Khasi Hills District, Meghalaya, India. *Egypt J Basic Appl Sci* 7:194–209. <https://doi.org/10.1080/2314808X.2020.1781747>
- Maden N, Akaryali E, Çelik N (2019) The in situ natural radionuclide (^{238}U , ^{232}Th and ^{40}K) concentrations in Gümüşhane granitoids: implications for radiological hazard levels of Gümüşhane city, northeast Turkey. *Environ Earth Sci* 78:330. <https://doi.org/10.1007/s12665-019-8333-x>
- Madruca MJ, Miró C, Reis M, Silva L (2019) Radiation Exposure from natural radionuclides in building materials. *Radiat Prot Dosimetry* 185(1):49–57
- Markkanen M (1995) Radiation dose assessments for materials with elevated natural radioactivity. STUK-B-STO, vol 32. Finnish Centre for Radiation and Nuclear Safety
- Marocchi M, Righi S, Maria Bargossi G, Gasparotto G (2011) Natural radionuclides content and radiological hazard of commercial ornamental stones: an integrated radiometric and mineralogical-petrographic study. *Radiat Meas* 46(5):538–545
- Martins LMO, Gomes MEP, Teixeira RJS, Pereira AJSC, Neves LJPF (2016) Indoor radon risk associated to post-tectonic biotite granites from Vila Pouca de Aguiar pluton, northern Portugal. *Ecotoxicol Environ Saf* 133:64–175. <https://doi.org/10.1016/j.ecoenv.2016.07.009>
- McBride EF (1963) A classification of common sandstones. *J Sediment Res* 33(3):664–669
- Moghazy NM, El-Tohamy AM, Fawzy MM, Awad HA, Zakaly HMM, Issa SAM, Ene A (2021) Natural radioactivity, radiological hazard and petrographical studies on Aswan granites used as building materials in Egypt. *Appl Sci* 11:6471. <https://doi.org/10.3390/app11146471>
- Mohamed RI, Algamdi SK, Al-shamani NS (2016) Evaluation of radionuclide concentrations and associated radiological hazard in marble indices and granite used as building materials in Al-Madinah Al-Munawarah. *J Taibah Univ Sci* 10(3):369–374
- Murphy K (2008) What's Lurking in Your Countertop. *The New York Times*. <https://www.nytimes.com/2008/07/24/garden/24granite.html>
- Murray EG, Adams JAS (1958) Thorium, uranium and potassium in some sandstones. *Geochim Cosmochim Acta* 13(4):260–269
- Myatt TA, Allen JG, Minegishi T, Mccarthy WB, Stewart JH, Macintosh DL, Mccarthy JF (2010) Assessing exposure to granite countertops—part 1: radiation. *J Exposure Sci Environ Epidemiol* 20(3):273–280
- Ngachin M, Garavaglia M, Giovani C, Nourreddine A, Njock MGK, Scruzzi E, Lagos L (2008) ^{226}Ra , ^{232}Th and ^{40}K contents and radon exhalation rate from materials used for construction and decoration in Cameroon. *J Radiol Prot* 28:369–378. <https://doi.org/10.1088/0952-4746/28/3/007>
- Nuccetelli C, Risica S, D'Alessandro M, Trevisi R (2012) Natural radioactivity in building material in the European Union: robustness of the activity concentration index I and comparison with a room model. *J Radiol Prot* 32:349
- Örgün Y, Altunsoy N, Şahin SY, Güngör Y, Gültekin AH, Karahan G, Karacık Z (2007) Natural and anthropogenic radionuclides in rocks and beach sands from Ezine region (Çanakkale), Western Anatolia. *Turkey Appl Radiat Isot* 65(6):739–747
- Pereira D, Neves L, Pereira A, Peinado M, Blanco JA, Tejado JJ (2012) A radiological study of some ornamental stones: the bluish granites from Extremadura (Spain). *Nat Hazard* 12(2):395–401
- Pereira A, Pereira D, Neves L, Peinado M, Armenteros I (2013) Radiological data on building stones from a Spanish region: Castilla y León. *Nat Hazard* 13(12):3493–3501
- Pereira A, Lamas R, Miranda M, Domingos F, Neves L, Ferreira N, Costa L (2017) Estimation of the radon production rate in granite rocks and evaluation of the implications for geogenic radon potential maps: a case study in Central Portugal. *J Environ Radioact* 166:270–277. <https://doi.org/10.1016/j.jenvrad.2016.08.022>
- Pettijohn FJ, Potter PE, Siever R (1987) Sand and sandstone. Springer, New York
- Pillai GS, Jeevarenuka K, Hameed PS (2017) Radioactivity in building materials of Pudukkottai Geological Region, Tamil Nadu, India. *Earth Syst Environ* 1:4. <https://doi.org/10.1007/s41748-017-0005-y>
- Plant JA, Saunders AD (1996) The radioactive earth. *Radiat Prot Dosimetry* 68(1):25–36
- Puccini A, Xhixha G, Cuccuru S, Oggiano G, Xhixha MK, Mantovani F, Alvarez CR, Casini L (2014) Radiological characterization of granitoid outcrops and dimension stones of the Variscan Corsica-Sardinia Batholith. *Environ Earth Sci* 71:393–405. <https://doi.org/10.1007/s12665-013-2442-8>
- Qureshi AA, Jadoon IAK, Wajid AA, Attique A, Masood A, Anees M, Manzoor S, Waheed A, Tubassam A (2014) Study of natural radioactivity in Mansehra granite, Pakistan: environmental

- concerns. *Radiat Prot Dosimetry* 158:466–478. <https://doi.org/10.1093/rpd/nct271>
- Rafique M, Khan AR, Jabbar A, Rahman SU, Kazmi SJA, Nasir T, Arshed W, Matiullah (2014) Evaluation of radiation dose due to naturally occurring radionuclides in rock samples of different origins collected from Azad Kashmir. *Russ Geol Geophys* 55(9):1103–1112
- Richter M, Jann O, Kemski J, Schneider U, Krockner C, Hoffmann B (2013) Determination of radon exhalation from construction materials using VOC emission test chambers. *Indoor Air* 23:397–405. <https://doi.org/10.1111/ina.12031>
- Rogers JJW, Richardson KA (1964) Thorium and uranium contents of some sandstones. *Geochim Cosmochim Acta* 28(12):2005–2011
- Sakoda A, Ishimori Y, Yamaoka K (2011) A comprehensive review of radon emanation measurements for mineral, rock, soil, mill tailing and fly ash. *Appl Radiat Isot* 69(10):1422–1435
- Sanjurjo-Sánchez J, Alves C (2017) Geologic materials and gamma radiation in the built environment. *Environ Chem Lett* 15:561–589. <https://doi.org/10.1007/s10311-017-0643-1>
- Sawhney BL (1972) Selective sorption and fixation of cations by clay minerals: a review. *Clays Clay Miner* 20(2):93–100
- Sayın N (2013) (2013) Radioactive element contents of some granites used as building materials: insights into the radiological hazards. *Bull Eng Geol Environ* 72:579–587. <https://doi.org/10.1007/s10064-013-0525-0>
- Schwarz HP, Blackwell B, Goldberg P, Marks AE (1979) Uranium series dating of travertine from archaeological sites, Nahal Zin. *Israel Nat* 277(5697):558–560
- Sêco SL, Domingos FP, Pereira AJSC, Duarte LV (2020) Estimation of the radon production potential in sedimentary rocks: a case study in the Lower and Middle Jurassic of the Lusitanian Basin (Portugal). *J Environ Radioact* 220:106272
- Shohda AM, Draz WM, Ali FA, Yassien MA (2018) Natural radioactivity levels and evaluation of radiological hazards in some Egyptian ornamental stones. *J Radiat Res Appl Sci* 11(4):323–327
- Siedel H, Siegesmund S (2014) Characterization of stone deterioration on buildings. *Stone in architecture*. Springer, Berlin, Heidelberg, pp 349–414
- Siegesmund S, Sneath R (eds) (2014) *Stone in architecture: properties, durability*. Springer Science and Business Media
- Siegesmund S, Török Á (2014) *Building stones*. Stone in Architecture. Springer, Berlin, Heidelberg, pp 11–95
- Syed HS (1999) Comparison studies adsorption of thorium and uranium on pure clay minerals and local Malaysian soil sediments. *J Radioanal Nucl Chem* 241(1):11–14
- Syuryavin AC, Park S, Nirwono MM, Lee SH (2020) Indoor radon and thoron from building materials: analysis of humidity, air exchange rate, and dose assessment. *Nucl Eng Technol* 52(10):2370–2378
- Taylor SR (1964) Abundance of chemical elements in the continental crust: a new table. *Geochim Cosmochim Acta* 28(8):1273–1285
- Tilling RI, Gottfried D (1969) Distribution of thorium, uranium, and potassium in igneous rocks of the boulder Batholith region, Montana, and its bearing on radiogenic heat production and heat flow. US Geological Survey Professional Paper
- Todorovic N, Bikit I, Krmar M, Mrdja D, Hansman J, Nikolov J, Forkapic VM, Bikit K, Jakonic I (2015) Natural radioactivity in raw materials used in building industry in Serbia. *Int J Environ Sci Technol* 12:705–716. <https://doi.org/10.1007/s13762-013-0470-2>
- Trevisi R, Risica S, D'Alessandro M, Paradiso D, Nuccetelli N (2012) Natural radioactivity in building materials in the European Union: a database and an estimate of radiological significance. *J Environ Radioact* 105:11–20
- Turhan S (2012) Estimation of possible radiological hazards from natural radioactivity in commercially-utilized ornamental and countertops granite tiles. *Ann Nucl Energy* 44:34–39. <https://doi.org/10.1016/j.anucene.2012.01.018>
- Turhan S, Aykamis AS, Kilic AM (2009) Natural radionuclide content and radiological hazard associated with usage of quartzite sand samples from Ovacik-Silifke-Mersin open pit as building material in Turkey. *Radiat Prot Dosimetry* 136(2):101–107
- Turhan S, Atci E, Varinlioğlu A (2015) Radiometric analysis of volcanic tuff stones used as ornamental and structural building materials in Turkey and evaluation of radiological risk. *Radioprotection* 50(4):273–280
- Tzortzis M, Tsertos H, Christofides S, Christodoulides G (2003) Gamma radiation measurements and dose rates in commercially-used natural tiling rocks (granites). *J Environ Radioact* 70(3):223–235
- US EPA (1993) Radon mitigation standards. US Environmental Protection Agency
- Weng P-S (1996) Distribution of naturally occurring radionuclides in the mountainous areas in Taiwan. *Environ Int* 22:49–54
- WHO (2009) WHO Handbook on indoor radon. A public health perspective. WHO Library Cataloguing-in-Publication Data
- NLM Classification, WN 615. World Nuclear Association. (2020). *Geology of Uranium Deposits*. Uranium Resources. https://apps.who.int/iris/bitstream/handle/10665/44149/9789241547673_eng.pdf;jsessionid=776D7E1EDB7AF15072BD1AA35EF83903?sequence=1
- World Nuclear Association (2020) *Geology of Uranium Deposits*. Uranium Resources. <https://world-nuclear.org/information-library/nuclear-fuel-cycle/uranium-resources/geology-of-uranium-deposits.aspx>
- Yalcin F, Ilbeyli N, Demirebilek M, Yalcin MG, Gunes A, Kaygusuz A, Ozmen SF (2020) Estimation of natural radionuclides' concentration of the Plutonic Rocks in the Sakarya Zone, Turkey using multivariate statistical methods. *Symmetry* 12(6):1048
- Yang Y, Saiers JE, Xu N, Minasian SG, Tyliczszak T, Kozimor SA, Shuh DK, Barnett MO (2012) Impact of natural organic matter on uranium transport through saturated geologic materials: from molecular to column scale. *Environ Sci Technol* 46(11):5931–5938
- Zeghib S, Aydarous AS, Al-Qahtany A (2016) Radiological hazard assessment of raw granites from Ranyah, KSA. *J Geosci Environ Prot* 04(09):24–38

Publisher's Note Springer Nature remains neutral with regard to jurisdictional claims in published maps and institutional affiliations.